ANNUAL REVIEWS

Annual Review of Vision Science

Generating and Using Transcriptomically Based Retinal Cell Atlases

Karthik Shekhar[1] and Joshua R. Sanes[2]

[1]Department of Chemical and Biomolecular Engineering; Helen Wills Neuroscience Institute; and California Institute for Quantitative Biosciences, QB3, University of California, Berkeley, California 94720, USA; email: kshekhar@berkeley.edu

[2]Center for Brain Science and Department of Molecular and Cell Biology, Harvard University, Cambridge, Massachusetts 02138, USA; email: sanesj@mcb.harvard.edu

Annu. Rev. Vis. Sci. 2021. 7:43–72

First published as a Review in Advance on July 6, 2021

The *Annual Review of Vision Science* is online at vision.annualreviews.org

https://doi.org/10.1146/annurev-vision-032621-075200

Keywords

amacrine cell, bipolar cell, horizontal cell, Müller glia, photoreceptor, retinal ganglion cell

Abstract

It has been known for over a century that the basic organization of the retina is conserved across vertebrates. It has been equally clear that retinal cells can be classified into numerous types, but only recently have methods been devised to explore this diversity in unbiased, scalable, and comprehensive ways. Advances in high-throughput single-cell RNA sequencing (scRNA-seq) have played a pivotal role in this effort. In this article, we outline the experimental and computational components of scRNA-seq and review studies that have used them to generate retinal atlases of cell types in several vertebrate species. These atlases have enabled studies of retinal development, responses of retinal cells to injury, expression patterns of genes implicated in retinal disease, and the evolution of cell types. Recently, the inquiry has expanded to include the entire eye and visual centers in the brain. These studies have enhanced our understanding of retinal function and dysfunction and provided tools and insights for exploring neural diversity throughout the brain.

INTRODUCTION

Classification and characterization of neural cell types are crucial for understanding the structure, development, function, and dysfunction of neural circuits. Neurons have long been categorized into discrete groups (classes and types, as defined below) based on shared morphological, connectional, functional, and molecular properties, but efforts at categorization have been labor intensive, incomplete, and often biased. It has also been unclear whether classifications based on different criteria agree with each other. Over the past decade, however, the introduction of high-throughput methods for profiling morphology, physiology, and gene expression has raised the enticing possibility of generating a comprehensive and unified taxonomy of neural cell types (Yuste et al. 2020). Among these, we focus on methods for sequencing the transcriptome of thousands of individual single cells or nuclei in a single assay. These methods have been particularly useful, as they offer the highest throughput at the lowest cost, provide an arguably more quantitative and unbiased framework than other methods, and enable genetic access to specific cell types. Furthermore, computational approaches drawn from statistics and machine learning can be applied to large-scale data sets generated by single-cell (sc-) and single-nucleus (sn-) RNA sequencing (RNA-seq) to define neuronal types and their interrelationships; identify cell type–specific markers; and compare tissue regions, developmental stages, and species.

The retina was the first tissue to which high-throughput scRNA-seq was applied (Macosko et al. 2015). Ensuing efforts over the past five years have generated a cell atlas of cell types for the mouse retina and shown striking correspondence between cell types defined molecularly and types defined by structural and functional criteria that are arguably of greater interest to most neurobiologists. These studies have served as a foundation for analyzing the development of the mouse retina and its responses to injury; for generating retinal cell atlases from other species, including humans; for assessing genetic underpinnings of blinding diseases; and for extending the analysis to other parts of the visual system both within the eye and deeper in the brain (**Figure 1*a*,*b***). Our purposes in this review are to summarize these studies and to provide the experimental and computational background needed to appreciate them.

THE VERTEBRATE RETINA

The fundamental structure of the retina is remarkably conserved among vertebrates (Baden et al. 2020). Cells of six classes are arranged in three cellular layers, called nuclear layers (**Figure 1*c***). The outer layer [the outer nuclear layer (ONL)] contains rod and cone photoreceptors (PRs), which sense light. The middle layer [the inner nuclear layer (INL)] contains three classes of interneurons—horizontal cells (HCs), bipolar cells (BCs), and amacrine cells (ACs)—as well as the major retinal glial class, Müller glia (MG). The inner layer (the ganglion cell layer) contains retinal ganglion cells (RGCs), some ACs, and in some species additional glia—astrocytes and/or oligodendrocytes. The six conserved classes (PRs, HCs, BCs, ACs, RGCs, and MG) all arise from a single set of retinal progenitors, whereas other glial types (astrocytes, oligodendrocytes, and microglia) migrate into the retina from extraocular sites of origin (Cepko 2014).

The three nuclear layers are separated from each other by synaptic (plexiform) layers. PRs, HCs, and BCs form synapses in the outer plexiform layer (OPL), which separates the ONL from the INL. The interneurons process the information that they receive from PRs and deliver it to RGCs in the inner plexiform layer (IPL), within which BCs, ACs, and RGCs form synapses. Axons of RGCs then send visual information to the rest of the brain through the optic nerve (**Figure 1*a–c***).

The cardinal principle of retinal function is that whereas PRs are light detectors (albeit very sophisticated ones), RGCs are feature detectors that are selectively responsive to specific patterned

stimuli such as oriented objects, movement in particular directions, or color contrasts (Masland 2012). This transformation of raw visual input into processed features results from information processing in the INL and selective connectivity between interneurons and RGCs. Specificity arises from the fact that there are many interneuronal types, each of which performs distinct computations and delivers its signals to distinct subsets of RGC types via synapses in the IPL. The specificity of these connections, along with some intrinsic differences among RGCs, results in each type responding preferentially to small subsets of visual features. Thus, the optic nerve actually carries a set of parallel representations of the visual field to the rest of the brain for further processing (Gollisch & Meister 2010, Sanes & Masland 2015). Although it has been known

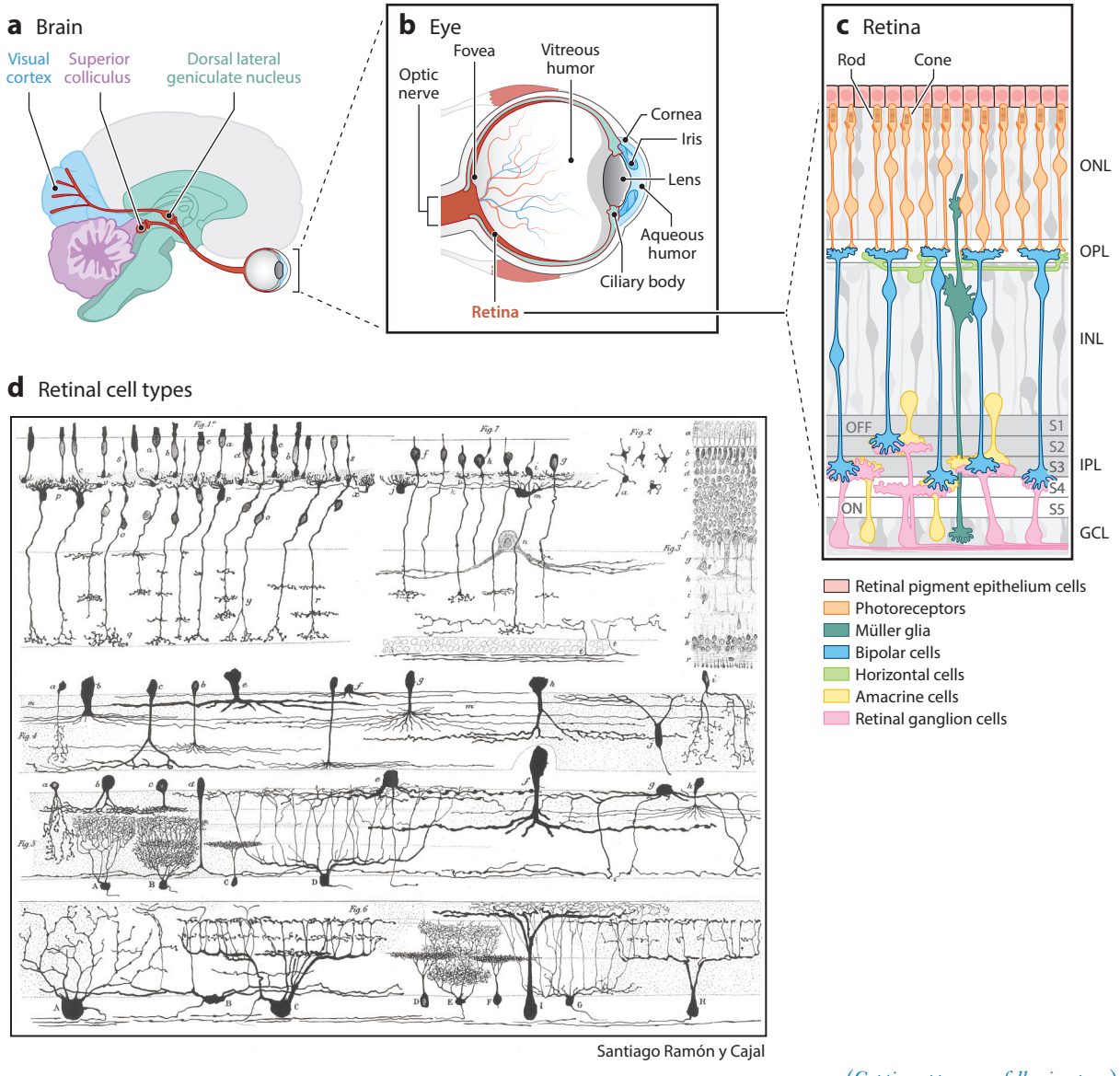

Santiago Ramón y Cajal

(*Caption appears on following page*)

Figure 1 (*Figure appears on preceding page*)

The vertebrate visual system. (*a*) The components of the visual system. Visual information from the eye is conveyed via the optic nerve to two primary relay regions located in the thalamus, the dorsal lateral geniculate nucleus and the superior colliculus. Dorsal lateral geniculate nucleus neurons project axons to layer 4 of the primary visual cortex. (*b*) The anatomy of the eye, with major tissues highlighted. Light enters via the cornea, the transparent front part of the eye, and is focused by the lens onto the retina, the light-sensitive neural tissue that lines the back of the eye. A central retinal region, the fovea, subserves most high-acuity vision; among mammals, it is present only in primates. The iris controls the amount of light entering the eye, while the ciliary body controls the shape of the lens. Output axons from the retina convey visual information to the rest of the brain via the optic nerve. The aqueous humor is a transparent gelatinous fluid that fills the anterior and posterior chambers of the eye surrounding the lens. The vitreous humor fills the space between the lens and the retina. The ciliary body controls the production of both the aqueous and vitreous humors. (*c*) Cross-section of the vertebrate retina showing its major cell classes: photoreceptors (i.e., rods and cones), horizontal cells, bipolar cells, amacrine cells, retinal ganglion cells, and Müller glia. The outer segments of the photoreceptors are embedded in retinal pigment epithelium cells that provide a variety of support functions. Photoreceptors, bipolar cells, and horizontal cells form synapses in the OPL, while bipolar cells, amacrine cells, and retinal ganglion cells form synapses in the IPL. The processes of each bipolar cell, amacrine cell, or retinal ganglion cell are confined to one or a few among five sublaminae within the IPL (S1–S5). Axons of retinal ganglion cells extend through the optic nerve to the midbrain. (*d*) Diverse morphologies of retinal neuronal types drawn by Santiago Ramón y Cajal (1892). Abbreviations: dLGN, dorsal lateral geniculate nucleus; GCL, ganglion cell layer; INL, inner nuclear layer; IPL, inner plexiform layer; ONL, outer nuclear layer; OPL, outer plexiform layer.

since the pioneering studies of Ramón y Cajal (1892) that retinal cell classes are divided into multiple, discrete types (**Figure 1*d***), systematic inventories of these types have only recently been assembled—thanks in large part to the advent of scRNA-seq.

Before proceeding, we note the distinctions among cell classes, subclasses, and types (Zeng & Sanes 2017) that we use throughout. Groups of cells that broadly share functional, structural, and molecular properties are called classes. As noted above, for the retina, the classes are PRs, HCs, BCs, ACs, RGCs, and MG. No one could mistake one class for another. At the other extreme, the smallest discrete groups that can be clearly distinguished from each other within a class are called types. The concept of types is not inconsistent with the fact that no two neurons are completely identical; division of cells into types necessarily ignores continuous variation, for example, in size or position, and emphasizes discontinuities that enable qualitative distinctions. Between types and classes are subclasses, which are useful in grouping types into families with shared features (see, for example, **Figure 2*f***).

SINGLE-CELL AND SINGLE-NUCLEUS RNA SEQUENCING: EXPERIMENTAL METHODS

History

The transcriptome of a cell, defined as the complete set of messenger RNA (mRNA) species and their individual quantities, encodes major swaths of the cell's molecular identity. Single-cell transcriptomic analysis is therefore a powerful approach to link phenotypes to genotypes and to compare phenotypes and genotypes across regions, developmental stages, or physiological conditions. Strategies for single-cell transcriptomic profiling were pioneered by two groups in the early 1990s who converted mRNA in individual cells to a complementary DNA (cDNA) library, amplified the resulting libraries, and used them to measure expression levels of candidate genes via probe-based hybridization (Brady et al. 1990, Eberwine et al. 1992). More comprehensive analysis of single-cell libraries became possible once high-density cDNA microarrays were available (Tietjen et al. 2003). In parallel, methods were developed for RNA-seq, which relies on the direct sequencing of cDNA fragments followed by bioinformatic alignment and quantification (Wang et al. 2009). RNA-seq, which exploited methodological advances and cost reductions enabled by the Human Genome Project, was quickly adopted to produce high-quality genome-scale transcription maps

from populations of cells from many tissues. These two streams converged when RNA-seq advanced to single-cell resolution (Tang et al. 2009).

scRNA-seq was initially applied to groups of up to a few hundred cells. These methods were, and continue to be, valuable for detailed characterization of neural cells. They are, however, woefully inadequate for classifying cells in the nervous system, where it seemed likely a priori (and has now been demonstrated) that most regions contain 100 or more cell types. Starting in 2014, however, methods were devised that have made it possible to perform scRNA-seq at high throughput (Mereu et al. 2020). These strategies include robotic fluid handling (Jaitin et al. 2014); droplet-based microfluidics (Klein et al. 2015, Macosko et al. 2015, Zheng et al. 2017); dispersing cells to individual nanoliter-sized microwells (Gierahn et al. 2017); and split-pool methods in which cells

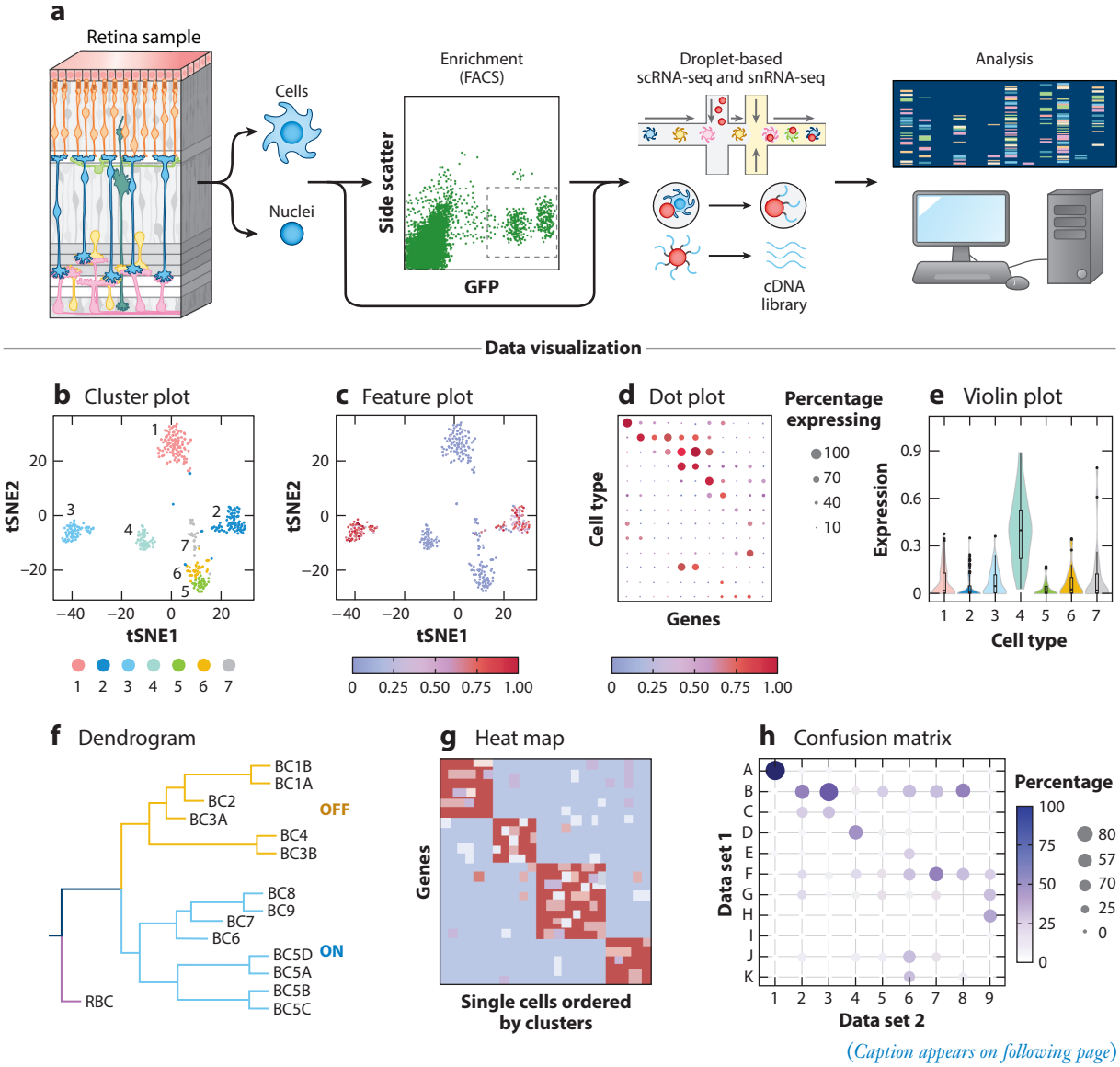

(*Caption appears on following page*)

Figure 2 (*Figure appears on preceding page*)

Overview of high-throughput scRNA-seq. (*a*) Key steps in scRNA-seq and snRNA-seq profiling. The dissected retinal tissue is dissociated to yield a suspension of single cells or nuclei that can be enriched for specific subpopulations using FACS. The resulting suspension is then flowed through a microfluidic device where individual cells or nuclei are isolated and lysed in nanoliter-sized aqueous droplets, and their mRNA is captured on barcoded oligonucleotides. Reverse transcription and amplification steps result in generation of a cDNA library that is sequenced. The resulting data sets are analyzed using statistical and machine learning techniques to gain insight into cell type heterogeneity at the transcriptomic level. (*b–h*) Methods for visualizing scRNA-seq and snRNA-seq results. (*b*) Two-dimensional visualization of the molecular diversity of cells using tSNE (van der Maaten & Hinton 2008). Each dot corresponds to a cell, with transcriptionally similar cells being assigned proximal coordinates. Cells are colored based on their transcriptomically defined cluster identity. (*c*) The same as panel *b* but with cells colored by their expression level of a single DE gene selectively expressed by some cell types. This representation is known as a feature plot. (*d*) A dot plot showing expression patterns of genes across a set of transcriptomically defined cell clusters. The size of each dot represents the percentage of cells in the cluster expressing the gene, and the color saturation represents the normalized expression strength. (*e*) A violin plot showing expression levels (*y* axis) of a single gene across clusters (*x* axis). Each violin is a representation of the probability distribution of the expression levels within each cluster. Box and whisker plots within each violin show the median value (*black horizontal line*), interquartile range (*bars*), range (*vertical lines*), and outliers (*dots*). (*f*) A dendrogram calculated using hierarchical clustering shows transcriptional interrelationships between mouse retinal bipolar clusters (Shekhar et al. 2016). Major cell subclasses, corresponding to rod BCs, OFF cone BCs, and ON cone BCs, separate into clades (*colors*). (*g*) Heat map showing expression patterns of specific marker genes in single cells grouped by their cell clusters. (*h*) Confusion matrix showing transcriptional correspondence between two groups of cell types. Circles and colors indicate the proportion of cells of a given row cluster assigned to a corresponding column cluster by a classification algorithm trained on column clusters. Abbreviations: BC, bipolar cell; cDNA, complementary DNA; DE, differential expression; FACS, fluorescence-activated cell sorting; GFP, green fluorescent protein; mRNA, messenger RNA; scRNA-seq, single-cell RNA sequencing; snRNA-seq, single-nucleus RNA sequencing; tSNE, t-distributed stochastic neighbor embedding.

are iteratively combined, split, and recombined through multiple rounds of successive barcoding (Cao et al. 2017, Rosenberg et al. 2018).

Droplet-Based Single-Cell RNA Sequencing

Three droplet-based methods were developed nearly simultaneously: Drop-seq (Macosko et al. 2015), InDrop (Klein et al. 2015), and 10X/GemCode (Zheng et al. 2017). Thanks to their high throughput, low cost, and ease of implementation, they have become the method of choice for the majority of studies, including nearly all of the ones that we discuss in this review. Of these, the 10X platform was commercialized earliest and has been by far the most widely used (**https://www.10xgenomics.com**).

In droplet-based methods, cells are dissociated from tissues or cultures; in some cases, subsets of interest are labeled by transgenic or immunochemical methods and enriched by fluorescence-activated cell sorting (FACS) (**Figure 2*a***). The cells are then passed through a microfluidic device that generates an emulsion of nanoliter-sized aqueous droplets suspended in oil. In the droplets, single cells are paired with single microbeads (Macosko et al. 2015) or hydrogels (Klein et al. 2015, Zheng et al. 2017). The beads and hydrogels bear hundreds of thousands of oligonucleotides (oligos), each containing a poly-T sequence complementary to the poly-A that terminates most eukaryotic mRNAs. The cell is lysed within the droplet, releasing its mRNA, which hybridizes to the capture oligos; following this, the mRNA is reverse transcribed into cDNA. The product is a single pooled library that is then amplified and sequenced. Thus, low- and high-throughput scRNA-seq methods are similar in principle; the transformative advance in the latter is that thousands of transcriptomes are captured in a single pooled reaction, compared to hundreds of individual reactions being captured in the former. This critical difference led to a huge reduction in cost and an exponential scaling of cellular throughput in just a few years (Svensson et al. 2018).

The obvious problem that high-throughput methods needed to solve was assigning sequence reads, derived from transcripts, to their cells of origin. The key was to incorporate molecular barcoding. mRNA-capturing oligos in the microbeads or hydrogels generally contain sequences that

enable the mRNA molecules to be indelibly marked following capture and reverse transcription. One set of nucleotides, called a cell barcode, is unique to a microbead or hydrogel but common to all oligos attached to it. The cell barcode allows sequencing reads to be grouped by their cell of origin. The oligos often also contain a second sequence, known as a unique molecular identifier (UMI). The UMI is a random sequence unique to each oligo. Its purpose is to correct for biases that can arise when minuscule amounts of cDNA are amplified by polymerase chain reaction (PCR); each UMI is counted only once when transcripts are quantified. Further molecular barcoding strategies have more recently been used to multiplex samples and measure additional readouts (e.g., surface protein expression or spatial location) (Rodriques et al. 2019; Stoeckius et al. 2017, 2018).

Beyond Single-Cell RNA Sequencing

Despite its numerous strengths, scRNA-seq cannot be applied to some samples, for example, tissues that are difficult to dissociate (e.g., heavily myelinated adult brain) or that could not be processed within a few hours of death. In response to these limitations, methods were developed to isolate nuclei from frozen tissue and sequence intranuclear RNA (Habib et al. 2016, Lake et al. 2016). This variant, called snRNA-seq, has been increasingly used, particularly for postmortem human samples that could be frozen quickly for processing later (Slyper et al. 2020). Nuclei contain less mRNA than cytoplasm but enough to enable robust transcriptomic analysis. Although snRNA-seq is biased toward recently transcribed genes and unspliced transcripts, studies have demonstrated strong correlation between the data obtained from scRNA-seq and snRNA-seq performed on equivalent samples (Lake et al. 2017).

The innovations that underlie high-throughput transcriptomic profiling have now been adapted to assess other aspects of cellular phenotype, including chromatin accessibility (Lareau et al. 2021), chromatin conformation (Ramani et al. 2017), and axonal projection (Kebschull et al. 2016). Further progress has enabled multimodal measurements, wherein transcriptomes are measured simultaneously with surface protein expression (Stoeckius et al. 2017), lineage (Raj et al. 2018), neuronal activity (Fuzik et al. 2016), spatial location (Eng et al. 2019, Moffitt et al. 2018, Rodriques et al. 2019, Vickovic et al. 2019, Wang et al. 2018), interregional connectivity (Huang et al. 2020), or effects of genetic or pharmacological perturbations (Dixit et al. 2016, Jaitin et al. 2016, Srivatsan et al. 2020). Thus, the transcriptomic approaches to the retina that we review are poised to advance to a multi-omics level.

SINGLE-CELL AND SINGLE-NUCLEUS RNA SEQUENCING: COMPUTATIONAL METHODS

Analyzing Single-Cell and Single-Nucleus RNA Sequencing Data

scRNA-seq and snRNA-seq measurements generate extraordinarily large data sets that require several processing and analysis steps before they are useful to neurobiologists. The initial set of sequencing reads requires preprocessing, with the aim of extracting a gene expression matrix (GEM). The rows and columns of the GEM are genes and individual cells, respectively, with entries corresponding to gene abundance per cell. Preprocessing steps vary depending on the library preparation protocol, but a typical sequence is as follows: First, raw read data are processed to filter out low-quality reads and trim adapter sequences, barcodes, and poly-A stretches. Second, the trimmed reads are aligned to the genome in a manner that accounts for splicing (Baruzzo et al. 2017). Freely available alignment software such as FastQC (**http://www.bioinformatics.babraham.ac.uk/projects/fastqc/**) and RNA-SeQC (DeLuca et al. 2012) provide pre- and postalignment quality control metrics, such as base quality statistics,

uniquely mapped reads, fraction of reads mapping to annotated exons, introns and intergenic regions, 3′ bias, and sense versus antisense reads. These measures generate metrics of library quality that are useful in assessing how results should be—or if they should be—analyzed further. Third, the reads are grouped by their cell of origin using cell barcodes, and PCR biases are removed using UMIs, resulting in a filtered GEM for the data set. Several software packages are available to perform these analyses, such as Cellranger (**https://support.10xgenomics.com/single-cell-gene-expression/software/pipelines/latest/what-is-cell-ranger**); Drop-seq tools (**https://github.com/broadinstitute/Drop-seq/releases**); bustools (**https://bustools.github.io/about**); Alevin (**https://salmon.readthedocs.io/en/latest/alevin.html**); and more recently, a cloud-based platform named Cumulus (**https://cumulus.readthedocs.io/en/stable/**).

Once preprocessing is complete, the GEMs are further analyzed through a series of steps to characterize transcriptomic variation across cells. Of the multiple software packages that enable such analyses, the most widely used include Seurat (Satija et al. 2015) and SCANPY (Wolf et al. 2018), in the programming languages R and Python, respectively. Because noise arising from experimental and biological sources can mask biological variations of interest (Hie et al. 2020, Luecken & Theis 2019, Stegle et al. 2015), the GEMs are usually subjected to an initial round of filtering to remove low-quality cells and genes, cell doublets, and signals arising from ambient RNA, as well as imputing missing expression values in the GEM, data normalization and scaling, and the identification of highly variable genes for further analysis. An additional challenge at this early stage is to combine scRNA-seq data collected across multiple experiments, sequencing platforms, and physiological conditions, a process known as integration (Lopez et al. 2018, Stuart et al. 2019, Welch et al. 2019). Approaches for data integration have been reviewed by Stuart & Satija (2019).

Next, preprocessed and integrated GEMs are subjected to two additional procedures to identify molecularly distinct cell types in the data—dimensionality reduction and clustering. Dimensionality reduction aims to learn a compact set of composite features from the data, each of which pools information from multiple genes in the GEM that exhibit correlated expression. These methods, including principal component analysis (PCA) and non-negative matrix factorization, create a new representation of the data set in which the number of independent features describing each cell reduces from thousands of genes to <100 gene modules (Stein-O'Brien et al. 2019). This reduced representation can be used to quantify similarity among cells, which in turn allows grouping (clustering) of transcriptomically similar cells (Kiselev et al. 2019).

Once clusters have been defined, they can be compared in multiple ways. The most common is to identify genes that exhibit robust differences between two or more clusters of interest, a task known as differential expression (DE) analysis. DE analysis in scRNA-seq presents unique statistical challenges compared to similar analysis for bulk RNA-seq data, necessitating the use of novel methods (Finak et al. 2015, Soneson and Robinson 2018). The development of new methodologies for scRNA-seq analysis continues to be an active area of research (Hie et al. 2020, Lähnemann et al. 2020, Luecken & Theis 2019).

Visualization of Single-Cell and Single-Nucleus RNA Sequencing Data

To be useful, scRNA-seq and snRNA-seq data must be presented in ways that make the results and conclusions intuitively obvious. This requires reducing dimensionality while preserving key features of the complexity of the data. Several approaches have been developed for this purpose.

Visualizing transcriptomically related cells. Methods like PCA or non-negative matrix factorization reduce the dimensionality of the data from thousands to tens of features but are intractable to visualize in toto. Three nonlinear visualization algorithms provide an intuitively

comprehensible view of transcriptomic relationships of cells in which reduced data are projected into a scatter plot wherein each point corresponds to a cell, and the distances between cells reflects transcriptional dissimilarity (**Figure 2*b***). These methods—t-distributed stochastic neighbor embedding (tSNE) (van der Maaten & Hinton 2008), uniform manifold approximation (McInnes et al. 2018), and force-directed layouts (Fruchterman & Reingold 1991)—are highly effective and frequently used. The nonlinear nature of approaches such as tSNE, however, can introduce distortions that must be controlled through appropriate choice of parameters (Kobak & Berens 2019, Wattenberg et al. 2016).

Visualizing gene expression. Once cells have been grouped into clusters (putative cell types), it is common to assess the expression of genes of interest—either those nominated a priori or those that exhibit DE among clusters. Expression patterns of single or small numbers of genes can be displayed by overlaying them on clusters (**Figure 2*c***) or as violin plots (**Figure 2*e***), while patterns of multiple genes are more often visualized using expression dot plots (**Figure 2*d***) or heat maps (**Figure 2*g***). Dot plots and heat maps are also used to visualize gene expression differences between data sets (e.g., healthy versus injured).

Mapping relationships among cell types. Cellular heterogeneity in the nervous system is often hierarchical in nature. For example, retinal cells can be divided into glia and neurons; neurons into PR, HC, BC, AC, and RGC classes; BCs into ON versus OFF subclasses; and (in the mouse) ON BCs into five types. Hierarchical clustering performed on the average transcriptomic profiles of clusters is an effective approach to visualize transcriptomic interrelationships at different levels of resolution all at once. The output of hierarchical clustering is a dendrogram (**Figure 2*f***), a branching structure, whose terminal leaves represent cell types that are hierarchically merged into clades based on their transcriptomic similarity. The dendrogram also simplifies the task of determining whether relationships defined molecularly correspond to those that had been derived from morphological or physiological measurements.

Comparing data sets. As increasing numbers of scRNA-seq and snRNA-seq studies are conducted that span multiple tissue regions, species, technologies, and physiological conditions, it is becoming possible to assess conservation of results across data sets. This comparison is frequently performed using multiclass supervised classification approaches such as Random Forest and XGBoost (Breiman 2001, Chen & Guestrin 2016). The results of these comparisons are typically visualized using a type of dot plot with the ironic name confusion matrix, which illustrates the extent of transcriptomic correspondence between two sets of clusters (**Figure 2*b***).

MOUSE RETINAL CELL ATLAS

Initial attempts to classify retinal cells were purely morphological (Polyak 1957, Ramón y Cajal 1892). Around the middle of the twentieth century, they were augmented by physiological studies using species favorable for recording—e.g., frogs, rabbits, and cats (e.g., Barlow & Hill 1963, Granit 1952, Kuffler 1953, Lettvin et al. 1959)—and later by immunohistochemical studies. Over the past 30 years, given its advantages of molecular knowledge and genetic accessibility, emphasis has shifted to the mouse, enabling the use of transgenic animals to label specific retinal types with green fluorescent protein (GFP) or other reporters. The labeled cells could then be subjected to detailed morphological study; targeted for electrophysiological recording (e.g., Huberman et al. 2008, Kim et al. 2008, Wässle et al. 2009); and isolated for gene expression profiling, initially with microarrays (Kay et al. 2011, 2012). In parallel, the increasing sensitivity of these methods allowed profiling of some single retinal cells (Cherry et al. 2009, Roesch et al. 2008, Trimarchi et al. 2007),

although the high cost and low throughput limited the use of these methods for purposes of cell type classification.

Over the past few years, the situation has changed dramatically with the introduction of higher-throughput methods: serial section electron microscopy (Bae et al. 2018, Greene et al. 2016, Helmstaedter et al. 2013, Marc et al. 2013); optical imaging of neural activity and transmitter release (Baden et al. 2016, Franke et al. 2017); and scRNA-seq, our focus in this review. The combination of these methods is now providing satisfying classification and characterization of cell types in the mouse retina.

When Macosko et al. (2015) devised Drop-seq, they applied it first to the retina because the strong foundation of prior knowledge (ground truth) provided a means of optimizing and validating the method. They used unsupervised methods to group approximately 44,000 single cells into 39 clusters. They were able to assign each cluster to a known cell type or groups of related types, including 33 spanning the five canonical neuronal classes plus MG and five other non-neuronal types.

Although these results were gratifying, they were clearly insufficient in that the number of authentic retinal cell types had already been estimated to exceed 60, and all RGCs clustered together even though at least a dozen types had already been described (Masland 2012, Sanes & Masland 2015). The reason for this lack of resolution was that approximately 80% of retinal cells are rod PRs (Jeon et al. 1998), leaving too few of the less abundant but more diverse neuronal classes (BCs, ACs, and RGCs) to recover rare types or distinguish similar types from each other. Our group therefore set out to enrich BCs, RGCs, and ACs so that we could profile them in sufficient numbers.

We began with BCs because we expected them to be the simplest of the heterogeneous classes and therefore the most suitable for testing alternative strategies for clustering and validation. We enriched BCs using a transgenic line in which GFP was expressed under control of regulatory elements from the *Vsx2* (*Chx10*) gene, which is expressed in BCs and MG in the adult mouse retina (Shekhar et al. 2016). From >27,000 single-cell transcriptomes, of which >23,000 could be identified as BCs, we identified 15 BC types (**Figure 3*a***). We combined lentivirus-mediated sparse labeling with immunohistochemistry and fluorescence in situ hybridization for genes selectively associated with specific clusters to match molecular identity to morphology for all 15 types (**Figure 3*b–d***). The correspondence was excellent, revealing that the 15 types included all 13 types that had been identified by morphological and physiological analyses (Euler et al. 2014, Franke et al. 2017, Greene et al. 2016, Helmstaedter et al. 2013, Wässle et al. 2009) and two new types.

One novel type, called BC1B, was particularly noteworthy in that it was monopolar and therefore would likely have been classified as an AC rather than a BC by conventional criteria (**Figure 3*c***). Molecular profiling showed that BC1B expressed no canonical AC markers but all canonical BC markers and was transcriptomically related to the conventional BC1A type. Della Santina et al. (2016) identified this type independently in a transgenic line and showed that it also shares ultrastructural and physiological properties with other BCs. In fact, using markers identified through scRNA-seq, we showed that BC1B is initially conventionally bipolar, then retracts its dendrites during early postnatal life.

Our group then adapted this pipeline to classify RGCs (Tran et al. 2019; **Figure 3*e–b***) and ACs (Yan et al. 2020a). RGCs were enriched either by using a line in which yellow fluorescent protein was expressed under control of regulatory elements from the *Slc17a6* (which encodes the glutamate transporter VGlut2) gene or by labeling them with antibodies to Thy1 (also known as CD90); both VGlut2 and Thy1 are broadly expressed in the brain but selectively expressed by RGCs in the retina. From approximately 35,000 single-cell transcriptomes, Tran et al. (2019) identified 46 RGC types. Lacking a suitable class-specific marker for ACs, Yan et al. adopted a strategy of selective

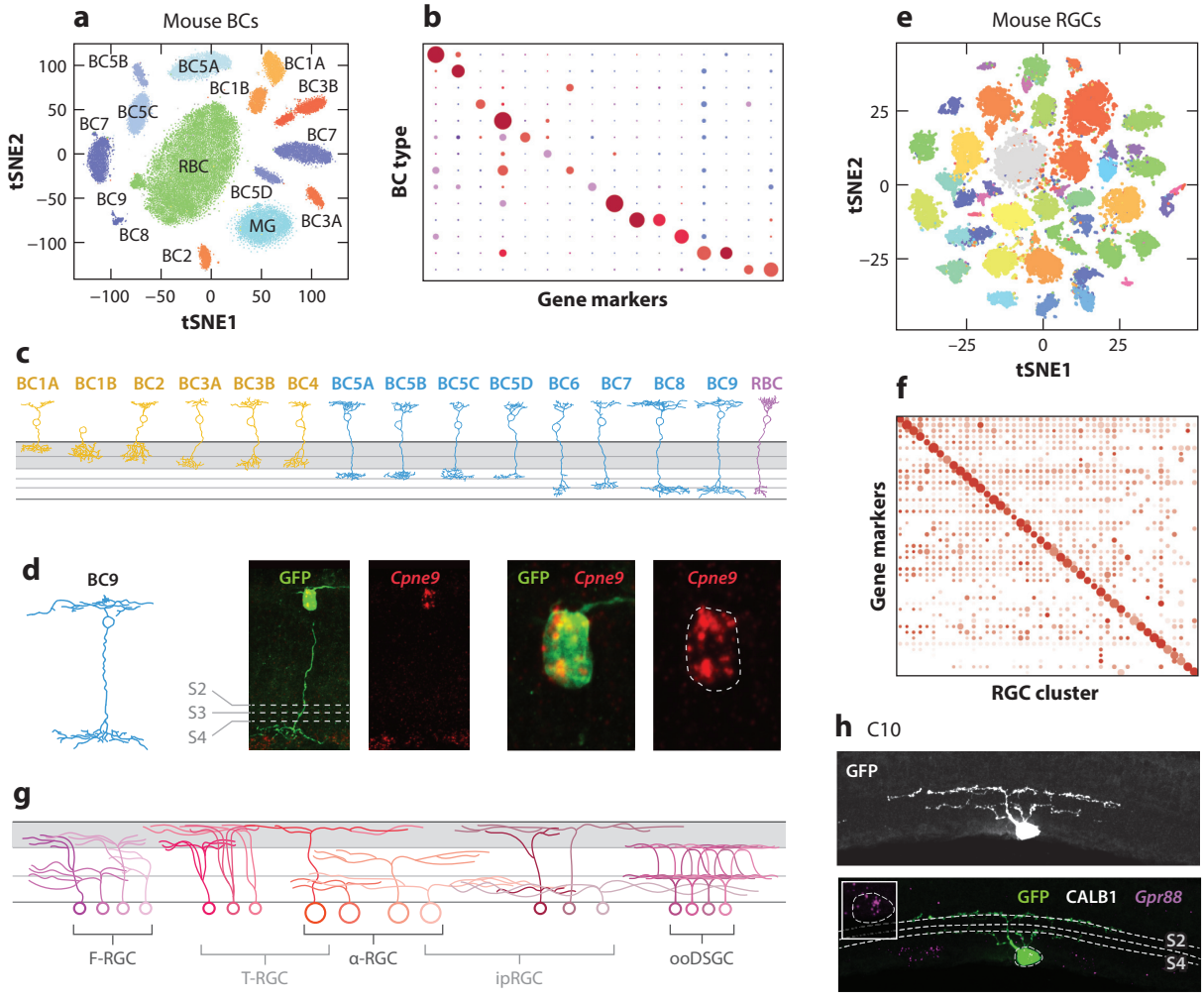

Figure 3

Classification of mouse BCs and RGCs. (*a*) Visualization of scRNA-seq data from mouse BC types and Müller glia using tSNE, as in **Figure 2*b***. (*b*) Genes selectively expressed by individual mouse BC types, shown in a dot plot as in **Figure 2*d***. (*c*) Morphologies of 15 mouse BC types. (*d*) Sparse labeling of a mouse BC (using lentivirus) combined with in situ hybridization for the type-specific marker *Cpne9* identifies this as BC9. The drawing on the left is from an electron microscopic reconstruction of a BC9 cell (Helmstaedter et al. 2013). Panels *a–d* adapted with permission from Shekhar et al. (2016). (*e*) Visualization of scRNA-seq data from mouse RGC clusters using tSNE. (*f*) Genes or gene pairs selectively expressed by individual mouse RGC types, shown in a dot plot. (*g*) Morphologies of several RGC types. (*h*) Sparse labeling of a mouse RGC (using a transgenic line) combined with in situ hybridization for *Gpr88* identifies this as RGC type C10. Dotted lines indicate the position of CALB2 staining, used to mark sublaminae in the IPL. Panels *e–h* adapted with permission from Tran et al. (2019). Abbreviations: BC, bipolar cell; GFP, green fluorescent protein; IPL, inner plexiform layer; RGC, retinal ganglion cell; scRNA-seq, single-cell RNA sequencing; tSNE, t-distributed stochastic neighbor embedding.

depletion, labeling BCs and MG (*vsx2-GFP*), and PRs (fluorophore-conjugated antibodies to CD73 and CD133), then collecting GFP/CD73/CD133 triple negative cells using FACS. From approximately 55,000 single cell transcriptomes, of which approximately 32,000 could be identified as ACs, they identified 63 AC types (Yan et al. 2020a). In nearly every case, it was possible to uniquely identify each type by selective expression of one gene or a combination of two genes

Table 1 Number of cell types in vertebrate retinas

Cell class	Mouse	Macaque (fovea)	Macaque (periphery)	Human (fovea)	Human (periphery)	Marmoset (fovea)	Marmoset (periphery)	Chick	Ferret	Zebrafish
Photoreceptors	3	4	4	4	4	3	3	8	3	5
Horizontal cells	1	2	2	2	2	2	2	4	2	ND
Bipolar cells	15	12	11	12	12	14	14	22	12	20
Amacrine cells	63	27	34	24	27	25	27	59	23	ND
Retinal ganglion cells	46	16	18	12	14	15	17	41	12	32
Müller glia	1	1	1	1	1	1	1	1	1	ND
Oligodendrocytes	0	0	0	0	0	0	0	1	ND	ND
Astrocytes	1	1	1	1	1	1	1	0	1	ND
Total	130	63	71	56	61	61	65	136	54	ND

Numbers were identified by scRNA-seq or snRNA-seq. For all species other than mice, numbers are likely to be underestimates owing to insufficient numbers of cells profiled. Data for the mouse taken from Macosko et al. (2015), Shekhar et al. (2016), Tran et al. (2019), and Yan et al. (2020a). Data for the macaque taken from Peng et al. (2019). Data for the human taken from Yan et al. (2020b). Data for zebrafish retinal ganglion cells taken from Kölsch et al. (2021). Data for zebrafish bipolar cells taken from Y. Kölsch, J. Hahn, K. Shekhar, J.R. Sanes and H. Baier (unpublished manuscript). Data for the chick taken from Yamagata et al. (2021). Data for the marmoset and ferret taken from Y. Peng, W. Yan and J.R. Sanes (unpublished manuscript). Abbreviations: ND, not determined; scRNA-seq, single-cell RNA sequencing; snRNA-seq, single-nucleus RNA sequencing.

and use these genes to elucidate the morphology of the type in question by combining in situ hybridization or immunohistochemistry with sparse labeling. Most recently, we have used similar methods to isolate and profile immune cells, including resident microglia (I. Benhar, J. Ding, K. Shekhar, A. Regev and J.R. Sanes, unpublished manuscript). Together, these efforts identified a total of 130 neuronal retinal types (**Table 1**) along with approximately 10 non-neuronal types, for a total of approximately 140.

As noted above, dendrograms can be used to display transcriptomic relationships of types within a class. In many cases, clades within these dendrograms show a gratifying correspondence to subclasses that had been proposed based on other criteria. For example, ON and OFF BC subclasses that respond to increases and decreases in light intensity, respectively, occupy separate clades (Shekhar et al. 2016) (**Figure 2*f***). Likewise, AC types that use GABA or glycine as the primary neurotransmitter and have largely distinct morphologies (wide-field arbors for GABAergic and narrow-field arbors for glycinergic) occupy separate clades. One can then seek transcription factors that correlate with, and might underlie, these distinctions. For example, *Meis2* is expressed at higher levels by most GABAergic AC types than by any glycinergic type, and *Tcf4* is expressed at higher levels by all glycinergic types than by any GABAergic type (Yan et al. 2020a). For RGCs, there is no obvious morphological or physiological signature of closely related types, but profiling identified transcriptionally proximate subclasses that share expression of transcription factors such as *Tbr1*, *Tbr2/Eomes*, *Neurod2*, and *Satb2* (Tran et al. 2019), some of which are known to affect the development of the RGC types that express them (Liu et al. 2018, Lyu & Mu 2021, Mao et al. 2014, Peng et al. 2017).

PRIMATE RETINAL CELL ATLAS

Although the mouse retina is an excellent system for studying the development, structure, and function of neural circuits, it has serious shortcomings as a model for human vision. This is because the retinas of primates, including humans, differ in important ways from those of rodents. Perhaps the most important is that primates, alone among mammals, have a small, specialized central retinal region called the fovea (**Figure 1*b***) that mediates most high-acuity as well as a

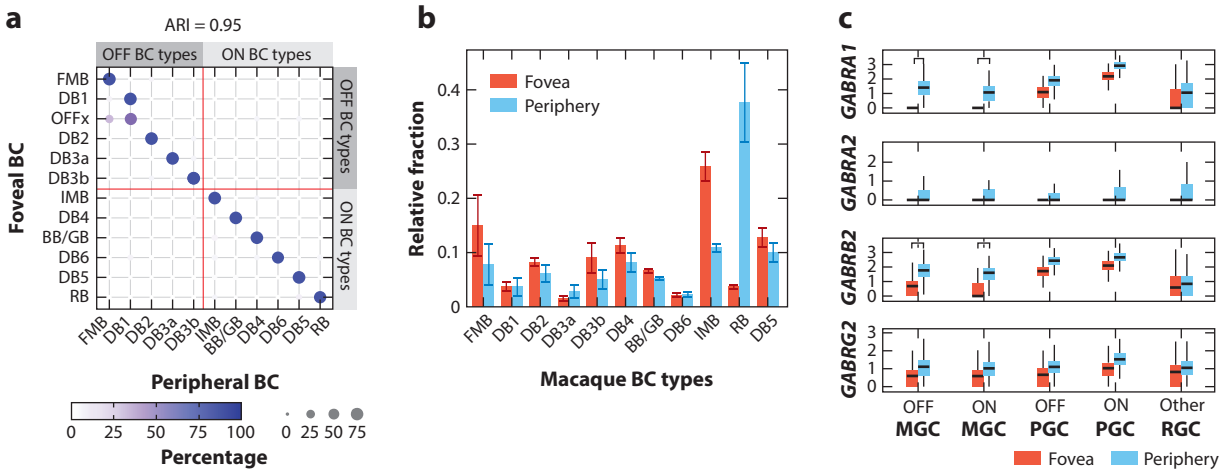

Figure 4

Cell types of the macaque fovea and peripheral retina. (*a*) Correspondence between BC types in the foveal and peripheral retina of the crab-eating macaque, shown as a confusion matrix, as in **Figure 2*b***. Bars on the top and right mark ON BC and OFF BC subclasses. The extent of 1:1 correspondence is quantified by the ARI (*top*), whose values range from 0 (random correspondence) to 1 (perfect match). (*b*) Comparison of relative proportions of matched BC types between the fovea and the periphery (mean ± standard deviation computed across biological replicates). (*c*) Box and whisker plots show that genes encoding subunits of receptors involved in GABAergic neurotransmission are expressed at higher levels in peripheral than in foveal RGCs. The black horizontal line represents the median; bars represent the interquartile range; vertical lines represent the minimum and maximum. Stars indicate >twofold change based on means. Figure adapted with permission from Peng et al. (2019). Abbreviations: ARI, adjusted Rand index; BC, bipolar cell; MGC, midget retinal ganglion cell; PGC, parasol retinal ganglion cell; RGC, retinal ganglion cell.

great deal of chromatic vision (Bringmann et al. 2018). The fovea occupies only approximately 1% of the retinal surface but provides approximately 50% of the input to the primary visual cortex. Moreover, diseases that selectively affect the fovea and the somewhat larger macula in which it is embedded are leading causes of irreversible vision loss—most notably age-related macular degeneration (AMD) and diabetic macular edema. Thus, crucial aspects of human retinal function and dysfunction cannot be satisfactorily studied in mice.

Peng et al. (2019) used the mouse atlas described above as a foundation to generate a retinal atlas from the macaque monkey, profiling the fovea and peripheral retina separately. Because the peripheral primate retina, like the mouse retina, is rod dominated, they enriched RGCs (using anti-Thy1) for some peripheral samples and depleted rods (using anti-CD73) from others to ensure detection of rare types. From approximately 170,000 single-cell transcriptomes, Peng et al. (2019) identified a total of 62 foveal and 70 peripheral cell types. They then asked the extent to which differences stem from cell types unique to one region, from altered proportions of the same set of types, or from region-specific molecular programs within shared types. They found that all three factors are involved but to different degrees. Most cell types exhibited a 1:1 correspondence between regions, but they identified a few region-specific cell types, including a novel foveal BC type that was named OFFx (**Figure 4*a***). Likewise, the proportions of cell types show regional variations, including some that had been documented previously, such as the higher fraction of cones and cone midget BCs and a lower fraction of rods and rod BCs in the fovea compared to the periphery (**Figure 4*b***). Shared types exhibited a median of 17 differentially expressed genes between the regions (with a range of 10–150) at log-fold change >2 (e.g., **Figure 4*c***). These differences presumably underlie many structural and functional differences between the two

regions and, as discussed below, may help explain why some retinal diseases preferentially target the macula.

Over the past two years, many groups have extended this analysis to the adult human retina, in many cases using the macaque atlas as a guide in assigning identities to clusters (Cherry et al. 2020, Cowan et al. 2020, Hamashima et al. 2020, Liang et al. 2019, Lukowski et al. 2019, Lyu et al. 2019, Menon et al. 2019, Orozco et al. 2020, Peng et al. 2019, Voigt et al. 2019b, Yan et al. 2020b, Yi et al. 2020). Unsurprisingly, and consistent with morphological and physiological studies, cell types in the macaque and human retina are very similar, as are their expression profiles. The number of types is slightly smaller in even the most complete human atlas (Yan et al. 2020b) compared to the macaque atlas (55 versus 60 in the fovea and 60 versus 70 in the peripheral retina), but this is more likely due to the lower number of cells profiled than to an authentic difference.

RETINAL DISEASE

Most irreversible vision loss results from retinal disease. There are several hundred retinal diseases. The three most prevalent, and the leading causes of irreversible vision loss worldwide, are AMD, diabetic retinopathy, and glaucoma. Monogenic causes account for an insignificant fraction of these, almost certainly <1%, and genome-wide association studies (GWASs) have identified over a hundred genes that affect susceptibility (e.g., Craig et al. 2020, Fritsche et al. 2016, Pollack et al. 2019). In contrast, monogenic causes have been identified for over 200 diseases that lead to dysfunction or loss of PRs, each of which is rare but which are substantial in aggregate; they have been classified into overlapping groups such as retinitis pigmentosa, cone–rod dystrophy, Leber congenital amaurosis, macular dystrophy, optic atrophy, macular telangiectasia, and inherited vitreoretinopathy (**https://sph.uth.edu/retnet/home.htm**).

Several groups have now used scRNA-seq and snRNA-seq data to inventory the macaque and human retinal cell types that express genes implicated in these diseases (Cowan et al. 2020, Lyu et al. 2019, Orozco et al. 2020, Peng et al. 2019, Yan et al. 2020b, Yi et al. 2020) (**Figure 5*a***). Unsurprisingly, many findings confirm previous conclusions based on clinical features and immunohistochemical results. For example, most genes that are mutated in retinitis pigmentosa, which initially affects rods, are selectively expressed by rods or by retinal pigment epithelial cells, which are required for rod viability. Likewise, most genes mutated in Leber hereditary optic neuropathies and autosomal dominant optic atrophies, which result in RGC death, are selectively expressed in RGCs; many susceptibility genes implicated in diabetic retinopathy, a predominantly microvascular complication of diabetes mellitus, are expressed in vascular endothelial cells (**Figure 5*b***).

However, many of the findings are new. Some genes mutated in retinitis pigmentosa or diabetic retinopathy are also expressed at high levels in RGCs or MG, perhaps accounting for otherwise perplexing clinical findings. *HTRA1*, a major susceptibility gene for macular degeneration, is expressed not only in pigment epithelium but also in horizontal cells and MG in both macaques and humans, suggesting potential additional sites of action (**Figure 5*c***). Complement pathway genes, also strongly implicated in macular degeneration, are expressed in a variety of cell types and classes in primates, as well as in mice (Pauly et al. 2019). Perhaps most enticing, several genes implicated in macular dystrophies, macular degeneration, and diabetic macular edema are expressed at higher levels by foveal than by peripheral cohorts of specific cell types, including PRs and vascular endothelium, providing starting points to investigate the increased susceptibility of the macula in these diseases.

Another way in which single-cell profiling can assist in understanding the pathogenesis of ocular disease is by allowing exploration of changes in cell types and gene expression patterns that correlate with disease. Few results of this type have been reported to date, but Voigt et al. (2020a)

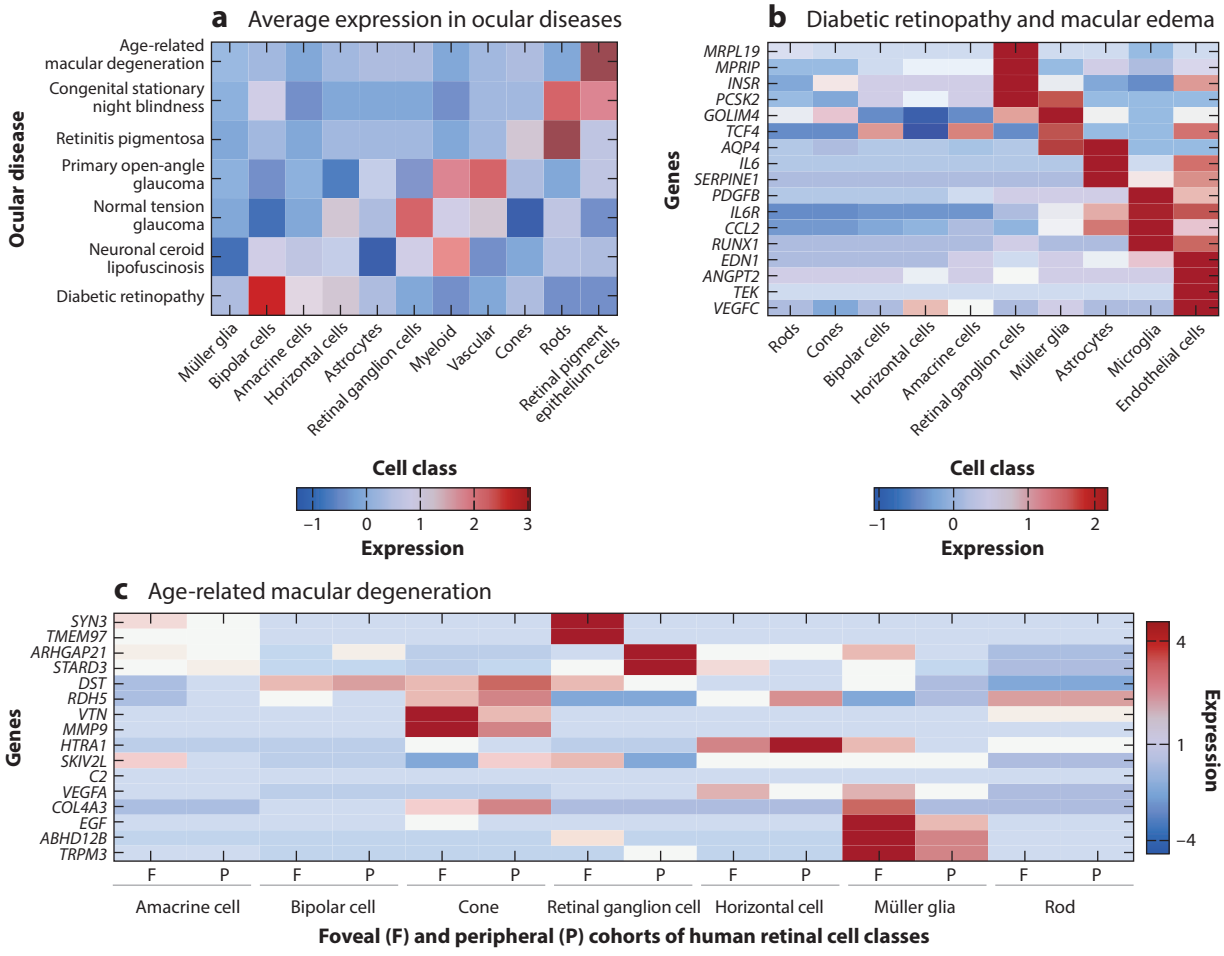

Figure 5

Retinal disease. (*a*) Heat map showing average expression strengths of well-known ocular disease susceptibility genes by cell classes in human retina single-nucleus RNA sequencing data. Panel adapted from Orozco et al. (2020) (CC BY 4.0). (*b*) Heat map showing relative expression of several genes implicated in diabetic retinopathy and macular edema by cell class. Panel adapted from Yan et al. (2020b) (CC BY 4.0). (*c*) Heat map showing relative expression of susceptibility genes for age-related macular degeneration in foveal and peripheral cohorts of human retinal cell classes. Panel adapted from Yi et al. (2020) (CC BY 4.0).

profiled retinal cells from four controls with little or no visual impairment and a single individual with autoimmune retinopathy, documenting alterations characteristic of gliosis in MG and astrocytes of the individual with retinopathy. Studies of mouse models of diabetic retinopathy (Van Hove et al. 2020) and inflammation (Bell et al. 2020) have also reported intriguing results.

INJURY

Following crush injury to the optic nerve [optic nerve crush (ONC)] in rodents, approximately 80% of RGCs die within two weeks, and only a few of the survivors extend new axons. Because the injury can be precisely controlled, can be applied to all RGCs simultaneously, and affects axons of all and only RGCs, ONC has become a much-used model to study mechanisms underlying

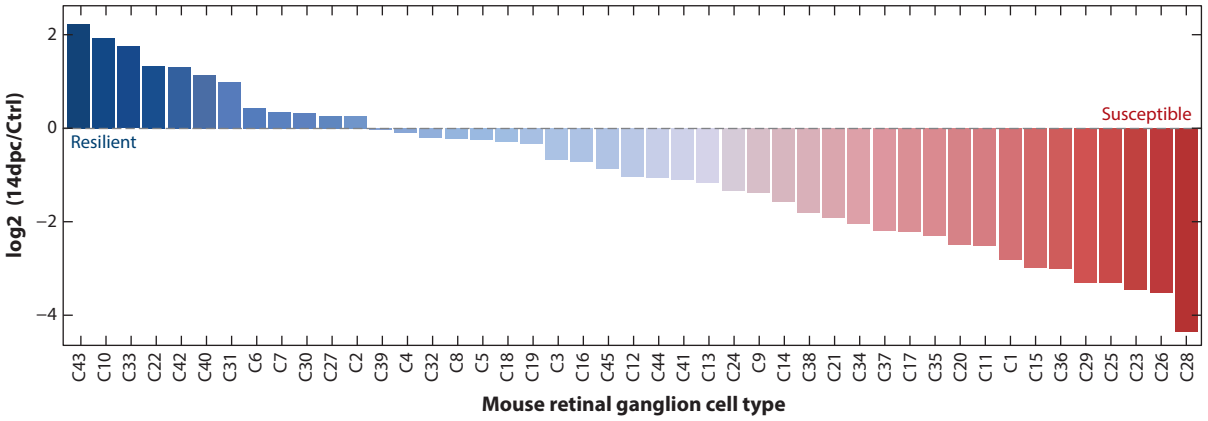

Figure 6

Resilience of mouse retinal ganglion cell types to injury (optic nerve crush) calculated as the frequency of each type 14 days after optic nerve crush (at which point approximately 80% of retinal ganglion cells have died) relative to their frequencies in uninjured retina. Retinal ganglion cell types exhibit a wide spectrum of survival at 14dpc, ranging from 1% to 98%. Figure adapted with permission from Tran et al. (2019).

injury and test interventions that could enhance survival or promote regeneration (Bray et al. 2019, Williams et al. 2020). ONC is also a valuable albeit severely limited model for studying mechanisms underlying glaucoma, in which RGCs die.

Two critical questions are (*a*) which RGCs live or die and (*b*) how surviving RGCs alter their gene expression profiles in response to injury. Initial studies using transgenic and immunohistochemical markers showed that survival is not stochastic, but rather differs among RGC types (de Sevilla Müller et al. 2014, Duan et al. 2015). Building on this result, Tran et al. (2019) used scRNA-seq to assess the vulnerability of all 46 RGC types. They profiled RGCs at multiple intervals following ONC and compared the frequency distribution of types in controls and following ONC.

A major challenge encountered in this study was that injury-related gene expression changes obscured the transcriptomic patterns on which cell-type identification was based. Tran et al. (2019) developed a computational approach, which they termed iGraphBoost, that leveraged the RGC profiles collected at intermediate time points to continually refine the transcriptional signatures that define each type. This allowed them to deconvolve gene signatures corresponding to cell type from injury-related alterations in cell state.

iGraphBoost analysis suggested that vulnerability varied dramatically among types, with survival ranging from 1% to 98% (**Figure 6**). This result raised the possibility that genes selectively expressed by or upregulated in resilient RGC types might be able to confer resilience on vulnerable types. Indeed, this turned out to be the case: Although no genes cleanly distinguished vulnerable from resilient types, many genes were selectively expressed in some but not all resilient or vulnerable types. In a few cases, Tran et al. (2019) were able to show that forced expression of resilience genes or inactivation of vulnerability genes in vulnerable types enhanced their survival. Moreover, in some of these cases, the intervention also enhanced the ability of surviving types to regenerate axons.

DEVELOPMENT

The vertebrate retina has been used in numerous studies of how diverse neural fates are acquired during early development (see, e.g., Bassett & Wallace 2012). All retinal cell classes can arise from

a single retinal progenitor cell (RPC) in sequential but overlapping birth windows (Cepko 2014, Young 1985). The currently leading model to explain these findings is one in which RPCs proceed through a series of competence states, in each of which they choose probabilistically from a set of possible fates, with the probability of each fate changing systematically as development proceeds. Thus, neuronal lineages in the vertebrate retina appear to be influenced by both deterministic and stochastic mechanisms, likely involving both cell-autonomous and extrinsic determinants (Cepko 2014, He et al. 2012).

Several transcriptomic studies have profiled the developing retina, beginning with bulk RNA measurements (Blackshaw et al. 2004, Hoshino et al. 2017, Mellough et al. 2019, Sajgo et al. 2017) or small numbers of single cells (Laboissonniere et al. 2017, Trimarchi et al. 2008) and moving to scRNA-seq in the mouse (Buenaventura et al. 2019, Clark et al. 2019, Giudice et al. 2019, Rheaume et al. 2018, Wu et al. 2021) and human retina (Hu et al. 2019, Lu et al. 2020, Sridhar et al. 2020). These studies have provided insights into key developmental regulators but suffer from an intrinsic limitation: Because RNA-seq is a destructive assay, the measurements represent a snapshot. Furthermore, retinal development is asynchronous (exhibiting, for example, a central-to-peripheral gradient), and cells from a single sample can span different stages of maturation. This pattern has led to the notion of pseudotime, which represents an unobserved dimension that measures a cell's progress along its fate (Trapnell et al. 2014). Algorithms have been developed for pseudotemporal ordering of single-cell transcriptomes, based on the reasonable assumption that transcriptomic similarity implies developmental proximity (Saelens et al. 2019). These methods can be used to construct developmental trajectories from longitudinal scRNA-seq snapshots, visualize developmental branchpoints, and pinpoint key genes that serve as fate determinants.

Clark et al. (2019) recently used this approach to analyze how cell classes arise in the mouse retina. They documented a progression beginning from primary RPCs (expressing *Pax6* and *Ccnd1*) that give rise to proliferating neurogenic cells (expressing the bHLH genes *Neurog2* and *Olig2*), which, in turn, give rise to branches corresponding to most of the major retinal neuronal classes (**Figure 7*a***). From this analysis, they were able to extract differentially expressed genes, including a set of three members of the NFI family of transcription factors (*Nfia*, *Nfib*, and *Nfix*), which they demonstrated, using in vivo experiments, are required for generation of late-born retinal cells. More recently, the same group reported parallel studies on human fetal retina and retinal organoids, pinpointing key differences between peripheral and macular development, as well as between mice and humans (Lu et al. 2020).

In contrast to our growing understanding of how retinal cell classes are generated, we know very little about how classes diversify into types. Indeed, the extent of type heterogeneity within classes was not fully appreciated when models of class lineage were formulated. As a first step in addressing this issue, our group enriched and profiled RGCs at multiple times, from when they first become postmitotic through adulthood (K. Shekhar, I.E. Whitney, S. Butrus and J.R. Sanes, unpublished manuscript). We find no evidence that 46 types of specified progenitors give rise to 46 RGC types. Instead, RGC type identity is acquired gradually, with progressive but incompletely deterministic restriction of fate (**Figure 7*c***). Diversification is not impacted by visual experience and largely independent of synaptic input, suggesting primary roles for cell-intrinsic factors and nonsynaptic cell–cell interactions.

ORGANOIDS

Organoids are complex cellular assemblies derived from embryonic or induced pluripotent stem cells (iPSCs) cultured by protocols that encourage self-organization into complex three-dimensional structures with multiple cell types; organoids differ fundamentally from the simpler

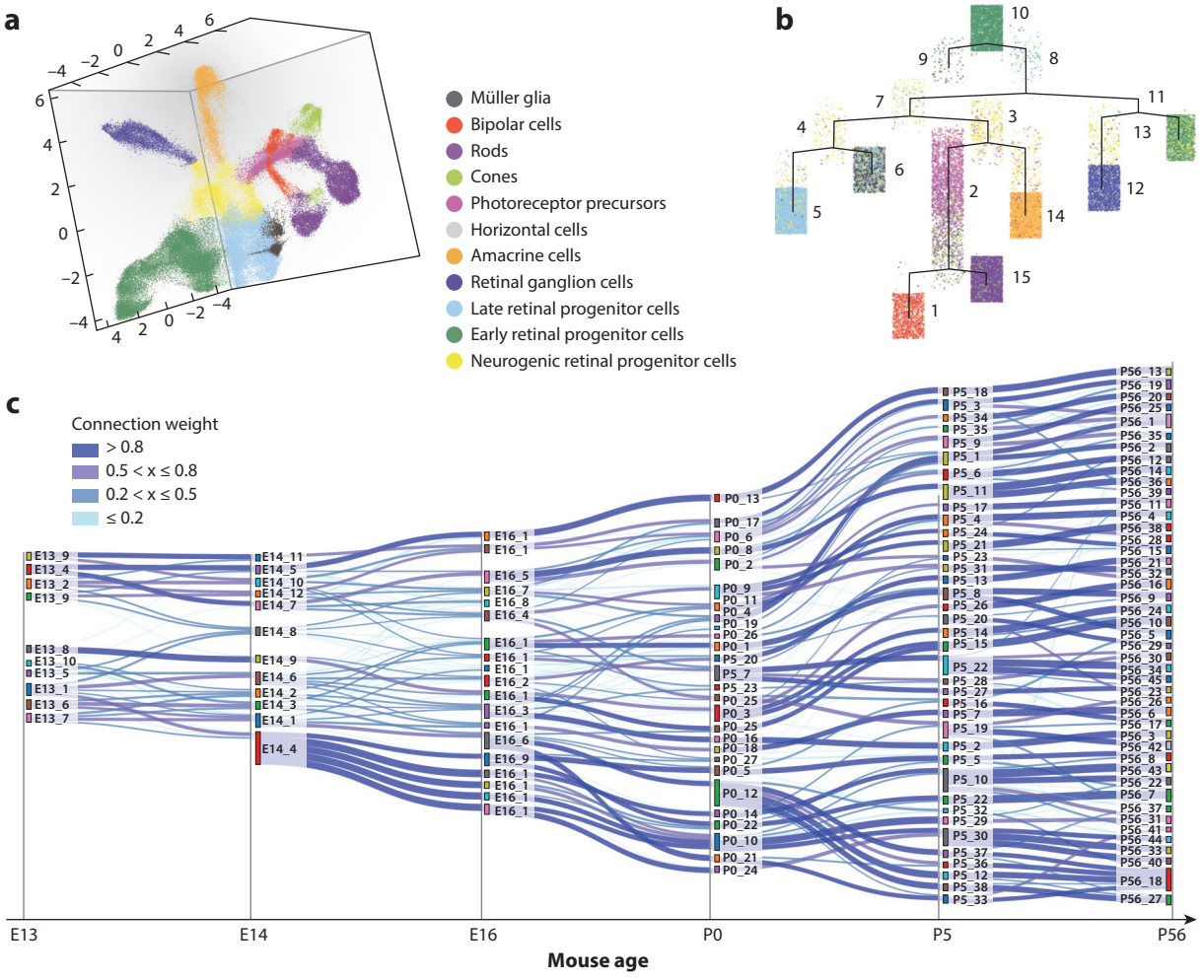

Figure 7

Retinal development. (*a*) Three-dimensional visualization of developing mouse retinal cells using uniform manifold approximation. Each transcriptomically defined cluster (*color*) has been assigned to a committed or immature retinal cell class based on its gene signatures. (*b*) Developmental relationships among clusters visualized as a tree using pseudotime analysis. (*c*) Temporal associations among immature retinal ganglion cell clusters (*y* axis) between consecutive ages (*x* axis) illustrated as a Sankey diagram. Nodes (*rectangles*) at each age correspond to transcriptionally defined clusters at each age (K. Shekhar, I.E. Whitney, S. Butrus and J.R. Sanes, unpublished manuscript). Edges depict transcriptional correspondences between clusters, with the color and thickness indicating the proportion of mappings that a late cluster (*right*) receives from an early cluster (*left*). Edge weights are normalized such that incoming edges add to 100%. Panels *a* and *b* adapted with permission from Clark et al. (2019).

and more homogeneous cultures that typically form when cells are cultured on conventional flat substrates. Among the first neural organoids to be generated were ones that recapitulated optic cup formation and included a multilayered retinal component (Eiraku et al. 2011). Since then, attention has been largely focused on improving methods to generate cerebral organoids (Del Dosso et al. 2020), but several groups have also reported protocols for generating retinal organoids, generally from iPSCs. In several cases, these organoids have been characterized by scRNA-seq (Collin et al. 2019, Cowan et al. 2020, Kim et al. 2019, Lu et al. 2020, Mao et al. 2019, O'Hara-Wright & Gonzalez-Cordero 2020, Sridhar et al. 2020).

Transcriptomic analysis confirms that all retinal cell classes are represented in these organoids. In general, they form in the same order as they do in vivo: RGCs form first, and PRs form later. As PRs form, RGCs in the interior die, likely because they are hypoxic and lack central targets. Thus, complete retinal circuits do not form in these structures, and in most cases, cells are so immature that it is unfeasible to ask whether diversification into types occurs. Recently, however, Cowan et al. (2020) devised improved protocols to generate organoids that do generate types within classes. Moreover, they used scRNA-seq to show that many types generated in organoids correspond to those observed in vivo. These results will enable generation of organoids from patient tissue, which can then be used to elucidate disease mechanisms and test interventions.

EVOLUTION

Many parts of the central nervous system, such as the cortex, differ in fundamental ways among vertebrates. In contrast, the basic plan of the retina—its three cellular layers, two synaptic layers, five neuronal classes, and MG—is conserved among all jawed vertebrates (Dowling 2012, Lamb et al. 2007) and even shares many design principles with the retina of *Drosophila* (Sanes & Zipursky 2010). Nonetheless, there are numerous species-specific variations on this common theme, possibly reflecting the needs of each species and the statistical properties of visual input in its ecological niche (Baden et al. 2020, Ocko et al. 2018). This combination of constancy and variability makes the retina ideal for evolutionary analysis of cell types. Just as genome sequencing enabled systematic identification of gene orthologies, assembling retinal atlases for different species can help build an evolutionary history of cell types (Marioni & Arendt 2017).

Until this year (2020), scRNA-seq and snRNA-seq studies of retina focused on mice, macaques, and humans. Recently, however, we and others have begun to assemble atlases of other mammalian species (the marmoset, ferret, pig, and deer mouse; K. Shekhar, W. Yan, J. Hahn, A. Monavarfeshani and J.R. Sanes, unpublished manuscript), as well as two nonmammalian vertebrates, the zebrafish and chick (Hoang et al. 2020, Kölsch et al. 2021, Yamagata et al. 2021). In both the chick and fish, CRISPR-Cas9-based approaches were used to label cell types based on their selective expression of specific genes identified via transcriptomic analysis to match molecularly defined types to morphology. Consistent with classical histological studies, retinas in both species appear to be at least as heterogeneous as those of mammals. For example, we identified 8 PRs, 4 HCs, and 22 BC types in the chick compared to 4, 2, and 12 in primates (**Table 1**).

These data sets can be used for evolutionary comparisons. One example is shown in **Figure 8*a***. In this case, all cells from the mouse, human, macaque, and chick atlases were combined and reanalyzed. Notably, transcriptomic similarity was greater among cells of a class than among cells of a species. Moreover, the dendrogram shows a hierarchy that fits with prior knowledge. The highest-level split is between MG and neurons; the second-highest separates photoreceptors from other neurons; the third-highest separates HCs from other interneurons and RGCs; and the lowest separates GABAergic from glycinergic ACs. With these results as a foundation, one can ask which gene expression programs are conserved among species and which vary.

A second example is shown in **Figure 8*b,c***, which displays relationships between mouse and macaque BCs and RGCs. While the correspondence is excellent for BCs, it is poor for RGCs. Also noteworthy is that the number of distinct RGC types in macaques is much lower than in mice (18 versus 46), with two types, the ON and OFF midget RGCs, accounting for nearly 85–90% of macaque RGCs. Disappointingly, the analysis failed to identify any convincing mouse orthologs of primate midget RGCs.

Based on these results, it is tempting to speculate that the outer retina may be composed of a conserved set of processers, with evolution acting primarily on inner retinal neuronal classes—ACs

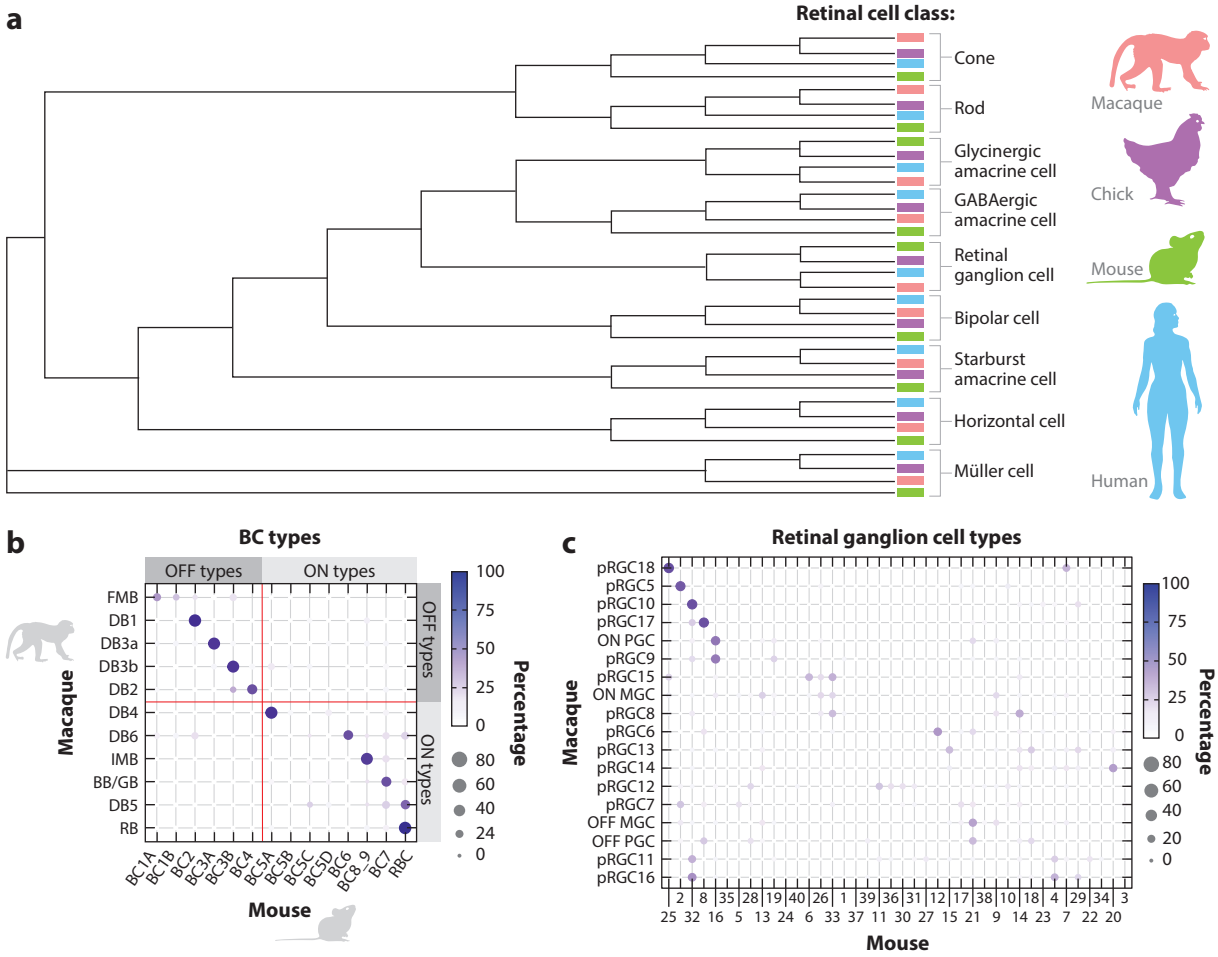

Figure 8

Retinal evolution. (*a*) Dendrogram illustrating the transcriptional relationships among retinal cell classes across four species—mouse, chick, human, and macaque. Photoreceptors have been subdivided into rods and cones; amacrine cells have been subdivided into GABAergic, glycinergic, and starburst subclasses. Panel adapted from Yamagata et al. (2021) (CC BY 4.0). (*b*) Confusion matrix showing transcriptomic correspondence between macaque and mouse BC types, with bars on the top and right marking OFF and ON BC subclasses, respectively. (*c*) Confusion matrix showing transcriptomic correspondence between macaque and mouse retinal ganglion cell clusters. Panels *b* and *c* adapted with permission from Peng et al. (2019).

and RGCs. A possible teleological explanation for this, based on comparing primates with mice, chicks, and fish, is that species with rudimentary cortices depend heavily on retinal computations, while primates rely more heavily on cortical processing.

THE REST OF THE EYE

Light enters the retina through the transparent cornea and lens, which focus the light and cast an inverted image on the retina (**Figure 1*b***). Also in the front of the eye are the iris, which controls the amount of light that enters, and an elaborate apparatus, including the ciliary body and trabecular meshwork, that controls intraocular pressure by regulating the production and drainage of

aqueous humor. Behind the retina, a layer of retinal pigment epithelial cells lies above the PRs, providing them with nutrient support, recycling visual pigment, and phagocytosing shed portions of outer segments. All of these tissues are of great clinical significance: For example, opacification of the lens results in cataracts, high intraocular pressure is the major modifiable risk factor for glaucoma, and dysfunction of the retinal pigment epithelium is the major contributor to AMD.

Over the past year, scRNA-seq methods have been applied to nonretinal ocular structures including the trabecular meshwork, lens, iris, cornea, choriocapillaris, and retinal pigment epithelium in mice (Bhat et al. 2019, Kaplan et al. 2019, Lehmann et al. 2020, van Zyl et al. 2020, Yu and Saban 2019) and humans (Hamashima et al. 2020; Patel et al. 2020; van Zyl et al. 2020; Voigt et al. 2019a, 2020b; T. van Zyl and J.R. Sanes, unpublished manuscript). One study compared human aqueous humor outflow pathways with those of four species commonly used to assess outflow mechanisms and test intraocular pressure modifying therapies—mice, two macaque species (*Macaca fascicularis* and *Macaca mulatta*), and pigs (van Zyl et al. 2020). Many cell types and marker genes were conserved among species, but others were not, suggesting the need for caution in extrapolating from model species to humans. These data sets have also been used to map expression of genes implicated in diseases such as glaucoma. Interestingly, several genes implicated in glaucoma accompanied by high intraocular pressure are expressed at higher levels in the trabecular meshwork than in RGCs, whereas the opposite is true for several genes implicated in normal tension glaucoma (Orozco et al. 2020, van Zyl et al. 2020). These results suggest a role for RGC-intrinsic variations in susceptibility to glaucoma.

BEHIND THE EYE

Axons of RGCs project to numerous retinorecipient areas in the brain—more than 40 in mice (Martersteck et al. 2017), many of which have been associated with distinct functions (Dhande et al. 2015). The two major retinorecipient areas are the optic tectum (called the superior colliculus in mammals) and the dorsal lateral geniculate nucleus (dLGN) in higher mammals (**Figure 1*a***). The optic tectum is the major area in lower mammals such as rodents and nonmammalian orders, whereas the dLGN is the major area in higher mammals such as primates. The dLGN provides the major visual input to the primary visual cortex, which then interconnects with numerous other visual cortical areas; an increasing proportion of RGC axons projecting to the dLGN rather than the superior colliculus correlates with the increasing size of the cortex. Researchers are beginning to use scRNA-seq and snRNA-seq to construct cell atlases of these regions of the visual system.

Subcortical Areas

A recent study reported transcriptomic classification of cell types in the mouse, macaque, and human dLGN (Bakken et al. 2020). Neurons separated cleanly into excitatory principal neurons and inhibitory interneurons in all three species. Excitatory neurons could be divided into multiple types in primates, with suggestive hints of heterogeneity in mice. These results are consistent with those of Kalish et al. (2018), who profiled the young postnatal mouse dLGN. To date, scRNA-seq or snRNA-seq studies of other retinorecipient areas have not been reported.

The Visual Cortex

Many studies have now used scRNA-seq or snRNA-seq to classify and characterize cell types in several mammalian species. Coverage of this growing area is beyond the scope of this review, but we note four landmark studies that provide insights into cell types of the visual cortex. One study compared the primary visual cortex with a motor cortical area (Tasic et al. 2018). It reported

a total of 111 neuronal types in visual cortex, 79 of which were shared with the motor cortex. Interestingly, conservation was greater among inhibitory interneurons than excitatory projection neurons, consistent with developmental evidence that projection neurons arise locally, whereas interneurons migrate from a single subcortical site. This paper also supports the contention that the retina is about as complex as other brain areas, at least as assessed by this criterion. Two subsequent studies from the same group showed strong correspondence between these transcriptomically defined types and those defined by morphological (intracellular filling) and electrophysiological (patch-clamping) criteria (Gouwens et al. 2019, 2020). Finally, Krienen et al. (2020) compared humans, macaques, marmosets, ferrets, and mice, providing initial insights into cell types unique to (or heavily enriched in) primates compared to other mammals.

CONCLUSIONS

The retina has been studied for two reasons that extend beyond its unquestionable beauty. First, as an unusually accessible part of the brain (Dowling 2012), it has served as a model to develop methods and elucidate mechanisms that can later be applied to less accessible regions. Second, since diseases of the retina and the eye that contains it underlie the vast majority of irreversible vision loss worldwide, developing an understanding of the cells at risk is of immense clinical significance.

Over the past five years, scRNA-seq and snRNA-seq have contributed to both aims. The strong foundation of prior knowledge about the mouse retina, as well as the availability of molecular and genetic tools, suited it for the development of a pipeline that could then be applied to other species, development, and disease. Success in molecular classification of retinal cell types has also been influential in addressing three questions relevant to neural classification more generally (Yuste et al. 2020).

First, can cells be divided into discrete types? This question has been debated for several reasons, including the difficulty of distinguishing between the type and state of a particular cell, which might be due to variations in activity, hormonal influence, circadian rhythm, and so on (Zeng & Sanes 2017). Indeed, in the forebrain, these and other factors may blur the distinction between type and state (Cembrowski & Spruston 2019, Kim et al. 2020, Stanley et al. 2020). Nonetheless, at least in the retina, types appear to be discrete, and the success of retinal classification has encouraged similar efforts in other regions of the mammalian brain (Yuste et al. 2020).

Second, do types defined molecularly correspond to types defined by the structural and functional criteria that guide most neurobiological thinking? For BCs, as noted above, there is a 1:1 correspondence between types identified from scRNA-seq-based atlases and types identified by high-throughput electron microscopic and electrophysiological methods. Characterization is less complete for ACs and RGCs, but to the extent that data are available, the correspondence is excellent (Baden et al. 2016, Bae et al. 2018, Franke et al. 2017, Greene et al. 2016; **http://rgctypes.org**). Thus, at least for the retina, there is little reason to doubt that transcriptome-based classification adequately captures classical distinctions among types.

Third, what is the best basis for neural classification? In the first days of high-throughput transcriptomics, there was fear that molecular distinctions would correspond poorly to morphological and physiological ones. Although, as we now know, correspondence is good, it is not perfect. Yet from an operational point of view, it is necessary to base categories on a single criterion. Although some dissenting opinions have been voiced (Vlasits et al. 2019), there is growing consensus that molecular criteria are to be favored: They have the highest throughput, are the easiest to quantify, can be studied in isolated cells, and lead directly to identification of genes that can be used to assess other features (Yuste et al. 2020). Molecules also provide perhaps the best starting point for investigating development, evolution, and disease. In contrast, functional measurements are less

objective and more context dependent, and high-throughput morphology is too labor intensive for general use.

Finally, with respect to disease and dysfunction, some initial steps have already been reported: The primate retinal and ocular atlases have already been used to assess expression of genes implicated in many visual disorders, comparing primate and mouse atlases has provided guidance on the extent to which the mouse eye can be used to model human disease, and the mouse atlas has served as a starting point to assess mechanisms of vulnerability to injury.

In conclusion, in just five years, high-throughput scRNA-seq and snRNA-seq have generated important resources and become broadly disseminated tools for studying the nervous system generally and the eye in particular. Over the next several years, we expect that these methods will increase in power and become increasingly useful for enhancing our knowledge of the structure, development, evolution, function, and dysfunction of the visual system.

DISCLOSURE STATEMENT

The authors are not aware of any affiliations, memberships, funding, or financial holdings that might be perceived as affecting the objectivity of this review.

ACKNOWLEDGMENTS

The authors would like to thank Maria del Carmen Diaz de la Loza for illustrations and figures. We are grateful to members of the Shekhar and Sanes labs for helpful discussions. Our studies have been supported by grants from the Chan Zuckerberg Initiative and National Institutes of Health (grants R00EY028625 to K.S. and R01EY022073 and R37NS029169 to J.R.S.) and by start-up funds from University of California at Berkeley.

LITERATURE CITED

Baden T, Berens P, Franke K, Rosón MR, Bethge M, Euler T. 2016. The functional diversity of retinal ganglion cells in the mouse. *Nature* 529:345–50

Baden T, Euler T, Berens P. 2020. Understanding the retinal basis of vision across species. *Nat. Rev. Neurosci.* 21:5–20

Bae JA, Mu S, Kim JS, Turner NL, Tartavull I, et al. 2018. Digital museum of retinal ganglion cells with dense anatomy and physiology. *Cell* 173:1293–306

Bakken TE, van Velthoven CT, Menon V, Hodge RD, Yao Z, et al. 2020. Single-cell RNA-seq uncovers shared and distinct axes of variation in dorsal LGN neurons in mice, non-human primates and humans. bioRxiv 367482. **https://doi.org/10.1101/2020.11.05.367482**

Barlow HB, Hill RM. 1963. Selective sensitivity to direction of movement in ganglion cells of the rabbit retina. *Science* 139:412–14

Baruzzo G, Hayer KE, Kim EJ, Di Camillo B, FitzGerald GA, Grant GR. 2017. Simulation-based comprehensive benchmarking of RNA-seq aligners. *Nat. Methods* 14:135–39

Bassett EA, Wallace VA. 2012. Cell fate determination in the vertebrate retina. *Trends Neurosci.* 35:565–73

Bell OH, Copland DA, Ward A, Nicholson LB, Lange CA, et al. 2020. Single eye mRNA-seq reveals normalisation of the retinal microglial transcriptome following acute inflammation. *Front. Immunol.* 10:3033

Bhat SP, Gangalum RK, Kim D, Mangul S, Kashyap RK, et al. 2019. Transcriptional profiling of single fiber cells in a transgenic paradigm of an inherited childhood cataract reveals absence of molecular heterogeneity. *J. Biol. Chem.* 294:13530–44

Blackshaw S, Harpavat S, Trimarchi J, Cai L, Huang H, et al. 2004. Genomic analysis of mouse retinal development. *PLOS Biol.* 2:e247

Brady G, Barbara M, Iscove NN. 1990. Representative in vitro cDNA amplification from individual hemopoietic cells and colonies. *Methods Mol. Cell Biol.* 2:17–25

Bray ER, Yungher BJ, Levay K, Ribeiro M, Dvoryanchikov G, et al. 2019. Thrombospondin-1 mediates axon regeneration in retinal ganglion cells. *Neuron* 103:642–57
Breiman L. 2001. Random forests. *Mach. Learn.* 45:5–32
Bringmann A, Syrbe S, Görner K, Kacza J, Francke M, et al. 2018. The primate fovea: structure, function and development. *Prog. Retin. Eye Res.* 66:49–84
Buenaventura DF, Corseri A, Emerson MM. 2019. Identification of genes with enriched expression in early developing mouse cone photoreceptors. *Investig. Ophthalmol. Vis. Sci.* 60:2787–99
Cao J, Packer JS, Ramani V, Cusanovich DA, Huynh C, et al. 2017. Comprehensive single-cell transcriptional profiling of a multicellular organism. *Science* 357:661–67
Cembrowski MS, Spruston N. 2019. Heterogeneity within classical cell types is the rule: lessons from hippocampal pyramidal neurons. *Nat. Rev. Neurosci.* 20:193–204
Cepko C. 2014. Intrinsically different retinal progenitor cells produce specific types of progeny. *Nat. Rev. Neurosci.* 15:615–27
Chen T, Guestrin C. 2016. Xgboost: a scalable tree boosting system. In *KDD '16: Proceedings of the 22nd ACM SIGKDD International Conference on Knowledge Discovery and Data Mining*, pp. 785–94. New York: ACM
Cherry TJ, Trimarchi JM, Stadler MB, Cepko CL. 2009. Development and diversification of retinal amacrine interneurons at single cell resolution. *PNAS* 106:9495–500
Cherry TJ, Yang MG, Harmin DA, Tao P, Timms AE, et al. 2020. Mapping the cis-regulatory architecture of the human retina reveals noncoding genetic variation in disease. *PNAS* 117:9001–12
Clark BS, Stein-O'Brien GL, Shiau F, Cannon GH, Davis-Marcisak E, et al. 2019. Single-cell RNA-seq analysis of retinal development identifies NFI factors as regulating mitotic exit and late-born cell specification. *Neuron* 102:1111–26
Collin J, Queen R, Zerti D, Dorgau B, Hussain R, et al. 2019. Deconstructing retinal organoids: single cell RNA-seq reveals the cellular components of human pluripotent stem cell-derived retina. *Stem Cells* 37:593–98
Cowan CS, Renner M, De Gennaro M, Gross-Scherf B, Goldblum D, et al. 2020. Cell types of the human retina and its organoids at single-cell resolution. *Cell* 182:1623–40
Craig JE, Han X, Qassim A, Hassall M, Cooke Bailey JN, et al. 2020. Multitrait analysis of glaucoma identifies new risk loci and enables polygenic prediction of disease susceptibility and progression. *Nat. Genet.* 52:160–66
de Sevilla Müller LP, Sargoy A, Rodriguez AR, Brecha NC. 2014. Melanopsin ganglion cells are the most resistant retinal ganglion cell type to axonal injury in the rat retina. *PLOS ONE* 9:e93274
Del Dosso A, Urenda JP, Nguyen T, Quadrato G. 2020. Upgrading the physiological relevance of human brain organoids. *Neuron* 107:1014–28
Della Santina L, Kuo SP, Yoshimatsu T, Okawa H, Suzuki SC, Hoon M, et al. 2016. Glutamatergic monopolar interneurons provide a novel pathway of excitation in the mouse retina. *Curr. Biol.* 26:2070–77
DeLuca DS, Levin JZ, Sivachenko A, Fennell T, Nazaire M-D, et al. 2012. RNA-SeQC: RNA-seq metrics for quality control and process optimization. *Bioinformatics* 28:1530–32
Dhande OS, Stafford BK, Lim J-HA, Huberman AD. 2015. Contributions of retinal ganglion cells to subcortical visual processing and behaviors. *Annu. Rev. Vis. Sci.* 1:291–328
Dixit A, Parnas O, Li B, Chen J, Fulco CP, et al. 2016. Perturb-Seq: dissecting molecular circuits with scalable single-cell RNA profiling of pooled genetic screens. *Cell* 167:1853–66
Dowling JE. 2012. *The Retina: An Approachable Part of the Brain*. Cambridge, MA: Harvard Univ. Press
Duan X, Qiao M, Bei F, Kim I-J, He Z, Sanes JR. 2015. Subtype-specific regeneration of retinal ganglion cells following axotomy: effects of osteopontin and mTOR signaling. *Neuron* 85:1244–56
Eberwine J, Yeh H, Miyashiro K, Cao Y, Nair S, et al. 1992. Analysis of gene expression in single live neurons. *PNAS* 89:3010–14
Eiraku M, Takata N, Ishibashi H, Kawada M, Sakakura E, et al. 2011. Self-organizing optic-cup morphogenesis in three-dimensional culture. *Nature* 472:51–56
Eng C-HL, Lawson M, Zhu Q, Dries R, Koulena N, et al. 2019. Transcriptome-scale super-resolved imaging in tissues by RNA seqFISH+. *Nature* 568:235–39
Euler T, Haverkamp S, Schubert T, Baden T. 2014. Retinal bipolar cells: elementary building blocks of vision. *Nat. Rev. Neurosci.* 15:507–19

Finak G, McDavid A, Yajima M, Deng J, Gersuk V, et al. 2015. MAST: a flexible statistical framework for assessing transcriptional changes and characterizing heterogeneity in single-cell RNA sequencing data. *Genome Biol*. 16:278

Franke K, Berens P, Schubert T, Bethge M, Euler T, Baden T. 2017. Inhibition decorrelates visual feature representations in the inner retina. *Nature* 542:439–44

Fritsche LG, Igl W, Bailey JN, Grassmann F, Sengupta S, et al. 2016. A large genome-wide association study of age-related macular degeneration highlights contributions of rare and common variants. *Nat. Genet.* 48:134–43

Fruchterman TM, Reingold EM. 1991. Graph drawing by force-directed placement. *Softw. Pract. Exp.* 21(11):1129–64

Fuzik J, Zeisel A, Máté Z, Calvigioni D, Yanagawa Y, et al. 2016. Integration of electrophysiological recordings with single-cell RNA-seq data identifies neuronal subtypes. *Nat. Biotechnol.* 34:175–83

Gierahn TM, Wadsworth MH, Hughes TK, Bryson BD, Butler A, et al. 2017. Seq-Well: portable, low-cost RNA sequencing of single cells at high throughput. *Nat. Methods* 14:395–98

Giudice QL, Leleu M, La Manno G, Fabre PJ. 2019. Single-cell transcriptional logic of cell-fate specification and axon guidance in early-born retinal neurons. *Development* 146:dev178103

Gollisch T, Meister M. 2010. Eye smarter than scientists believes: neural computations in circuits of the retina. *Neuron* 65:150–64

Gouwens NW, Sorensen SA, Baftizadeh F, Budzillo A, Lee BR, et al. 2020. Integrated morphoelectric and transcriptomic classification of cortical GABAergic cells. *Cell* 183:935–53.e19

Gouwens NW, Sorensen SA, Berg J, Lee C, Jarsky T, et al. 2019. Classification of electrophysiological and morphological neuron types in the mouse visual cortex. *Nat. Neurosci.* 22:1182–95

Granit R. 1952. Aspects of excitation and inhibition in the retina. *Proc. R. Soc. Lond. B* 140:191–99

Greene MJ, Kim JS, Seung HS. 2016. Analogous convergence of sustained and transient inputs in parallel on and off pathways for retinal motion computation. *Cell Rep.* 14:1892–900

Habib N, Li Y, Heidenreich M, Swiech L, Avraham-Davidi I, et al. 2016. Div-Seq: Single-nucleus RNA-Seq reveals dynamics of rare adult newborn neurons. *Science* 353:925–28

Hamashima K, Gautam P, Lau KA, Khiong CW, Blenkinsop TA, et al. 2020. Potential modes of COVID-19 transmission from human eye revealed by single-cell atlas. bioRxiv 085613. **https://doi.org/10.1101/2020.05.09.085613**

He J, Zhang G, Almeida AD, Cayouette M, Simons BD, Harris WA. 2012. How variable clones build an invariant retina. *Neuron* 75:786–98

Helmstaedter M, Briggman KL, Turaga SC, Jain V, Seung HS, Denk W. 2013. Connectomic reconstruction of the inner plexiform layer in the mouse retina. *Nature* 500:168–74

Hie B, Peters J, Nyquist SK, Shalek AK, Berger B, Bryson BD. 2020. Computational methods for single-cell RNA sequencing. *Annu. Rev. Biomed. Data Sci.* 3:339–64

Hoang T, Wang J, Boyd P, Wang F, Santiago C, et al. 2020. Gene regulatory networks controlling vertebrate retinal regeneration. *Science* 370:eabb8598

Hoshino A, Ratnapriya R, Brooks MJ, Chaitankar V, Wilken MS, et al. 2017. Molecular anatomy of the developing human retina. *Dev. Cell* 43:763–79

Hu Y, Wang X, Hu B, Mao Y, Chen Y, et al. 2019. Dissecting the transcriptome landscape of the human fetal neural retina and retinal pigment epithelium by single-cell RNA-seq analysis. *PLOS Biol.* 17:e3000365

Huang L, Kebschull JM, Fürth D, Musall S, Kaufman MT, et al. 2020. BRICseq bridges brain-wide interregional connectivity to neural activity and gene expression in single animals. *Cell* 182:177–88

Huberman AD, Manu M, Koch SM, Susman MW, Lutz AB, et al. 2008. Architecture and activity-mediated refinement of axonal projections from a mosaic of genetically identified retinal ganglion cells. *Neuron* 59:425–38

Jaitin DA, Kenigsberg E, Keren-Shaul H, Elefant N, Paul F, et al. 2014. Massively parallel single-cell RNA-seq for marker-free decomposition of tissues into cell types. *Science* 343:776–79

Jaitin DA, Weiner A, Yofe I, Lara-Astiaso D, Keren-Shaul H, et al. 2016. Dissecting immune circuits by linking CRISPR-pooled screens with single-cell RNA-seq. *Cell* 167:1883–96

Jeon C-J, Strettoi E, Masland RH. 1998. The major cell populations of the mouse retina. *J. Neurosci.* 18:8936–46

Kalish BT, Cheadle L, Hrvatin S, Nagy MA, Rivera S, et al. 2018. Single-cell transcriptomics of the developing lateral geniculate nucleus reveals insights into circuit assembly and refinement. *PNAS* 115:E1051–60

Kaplan N, Wang J, Wray B, Patel P, Yang W, et al. 2019. Single-cell RNA transcriptome helps define the limbal/corneal epithelial stem/early transit amplifying cells and how autophagy affects this population. *Investig. Ophthalmol. Vis. Sci.* 60:3570–83

Kay JN, Chu MW, Sanes JR. 2012. MEGF10 and MEGF11 mediate homotypic interactions required for mosaic spacing of retinal neurons. *Nature* 483:465–69

Kay JN, Voinescu PE, Chu MW, Sanes JR. 2011. Neurod6 expression defines new retinal amacrine cell subtypes and regulates their fate. *Nat. Neurosci.* 14:965–72

Kebschull JM, da Silva PG, Reid AP, Peikon ID, Albeanu DF, Zador AM. 2016. High-throughput mapping of single-neuron projections by sequencing of barcoded RNA. *Neuron* 91:975–87

Kim EJ, Zhang Z, Huang L, Ito-Cole T, Jacobs MW, et al. 2020. Extraction of distinct neuronal cell types from within a genetically continuous population. *Neuron* 107:274–82

Kim I-J, Zhang Y, Yamagata M, Meister M, Sanes JR. 2008. Molecular identification of a retinal cell type that responds to upward motion. *Nature* 452:478–82

Kim S, Lowe A, Dharmat R, Lee S, Owen LA, et al. 2019. Generation, transcriptome profiling, and functional validation of cone-rich human retinal organoids. *PNAS* 116:10824–33

Kiselev VY, Andrews TS, Hemberg M. 2019. Challenges in unsupervised clustering of single-cell RNA-seq data. *Nat. Rev. Genet.* 20:273–82

Klein AM, Mazutis L, Akartuna I, Tallapragada N, Veres A, et al. 2015. Droplet barcoding for single-cell transcriptomics applied to embryonic stem cells. *Cell* 161:1187–201

Kobak D, Berens P. 2019. The art of using t-SNE for single-cell transcriptomics. *Nat. Commun.* 10:5416

Kölsch Y, Hahn J, Sappington A, Stemmer M, Fernandes AM, et al. 2021. Molecular classification of zebrafish retinal ganglion cells links genes to cell types to behavior. *Neuron* 109:645–62

Krienen FM, Goldman M, Zhang Q, Del Rosario RC, Florio M, et al. 2020. Innovations present in the primate interneuron repertoire. *Nature* 586:262–69

Kuffler SW. 1953. Discharge patterns and functional organization of mammalian retina. *J. Neurophysiol.* 16:37–68

Laboissonniere LA, Martin GM, Goetz JJ, Bi R, Pope B, et al. 2017. Single cell transcriptome profiling of developing chick retinal cells. *J. Comp. Neurol.* 525:2735–81

Lähnemann D, Köster J, Szczurek E, McCarthy DJ, Hicks SC, et al. 2020. Eleven grand challenges in single-cell data science. *Genome Biol.* 21:31

Lake BB, Ai R, Kaeser GE, Salathia NS, Yung YC, et al. 2016. Neuronal subtypes and diversity revealed by single-nucleus RNA sequencing of the human brain. *Science* 352:1586–90

Lake BB, Codeluppi S, Yung YC, Gao D, Chun J, et al. 2017. A comparative strategy for single-nucleus and single-cell transcriptomes confirms accuracy in predicted cell-type expression from nuclear RNA. *Sci. Rep.* 7:6031

Lamb TD, Collin SP, Pugh EN. 2007. Evolution of the vertebrate eye: opsins, photoreceptors, retina and eye cup. *Nat. Rev. Neurosci.* 8:960–76

Lareau CA, Ludwig LS, Muus C, Gohil SH, Zhao T, et al. 2021. Massively parallel single-cell mitochondrial DNA genotyping and chromatin profiling. *Nat. Biotechnol.* 39:451–61

Lehmann GL, Hanke-Gogokhia C, Hu Y, Bareja R, Salfati Z, et al. 2020. Single-cell profiling reveals an endothelium-mediated immunomodulatory pathway in the eye choroid. *J. Exp. Med.* 217:e20190730

Lettvin J, Maturana H, McCulloch W, Pitts W. 1959. What the frog's eye tells the frog's brain. *Proc. IRE* 47:1940–51

Liang Q, Dharmat R, Owen L, Shakoor A, Li Y, et al. 2019. Single-nuclei RNA-seq on human retinal tissue provides improved transcriptome profiling. *Nat. Commun.* 10:5743

Liu J, Reggiani JD, Laboulaye MA, Pandey S, Chen B, et al. 2018. Tbr1 instructs laminar patterning of retinal ganglion cell dendrites. *Nat. Neurosci.* 21:659–70

Lopez R, Regier J, Cole MB, Jordan MI, Yosef N. 2018. Deep generative modeling for single-cell transcriptomics. *Nat. Methods* 15:1053–58

Lu Y, Shiau F, Yi W, Lu S, Wu Q, et al. 2020. Single-cell analysis of human retina identifies evolutionarily conserved and species-specific mechanisms controlling development. *Dev. Cell* 53:473–91

Luecken MD, Theis FJ. 2019. Current best practices in single-cell RNA-seq analysis: a tutorial. *Mol. Syst. Biol.* 15:e8746

Lukowski SW, Lo CY, Sharov AA, Nguyen Q, Fang L, et al. 2019. A single-cell transcriptome atlas of the adult human retina. *EMBO J.* 38:e100811

Lyu J, Mu X. 2021. Genetic control of retinal ganglion cell genesis. *Cell. Mol. Life Sci.* 78:4417–33

Lyu Y, Zauhar R, Dana N, Strang CE, Wang K, et al. 2019. Integrative single-cell and bulk RNA-seq analysis in human retina identified cell type-specific composition and gene expression changes for age-related macular degeneration. bioRxiv 768143. **https://doi.org/10.1101/768143**

Macosko EZ, Basu A, Satija R, Nemesh J, Shekhar K, et al. 2015. Highly parallel genome-wide expression profiling of individual cells using nanoliter droplets. *Cell* 161:1202–14

Mao CA, Li H, Zhang Z, Kiyama T, Panda S, et al. 2014. T-box transcription regulator Tbr2 is essential for the formation and maintenance of Opn4/melanopsin-expressing intrinsically photosensitive retinal ganglion cells. *J. Neurosci.* 34:13083–95

Mao X, An Q, Xi H, Yang X-J, Zhang X, et al. 2019. Single-cell RNA sequencing of hESC-derived 3D retinal organoids reveals novel genes regulating RPC commitment in early human retinogenesis. *Stem Cell Rep.* 13:747–60

Marc RE, Jones BW, Watt CB, Anderson JR, Sigulinsky C, Lauritzen S. 2013. Retinal connectomics: towards complete, accurate networks. *Prog. Retin. Eye Res.* 37:141–62

Marioni JC, Arendt D. 2017. How single-cell genomics is changing evolutionary and developmental biology. *Annu. Rev. Cell Dev. Biol.* 33:537–53

Martersteck EM, Hirokawa KE, Evarts M, Bernard A, Duan X, et al. 2017. Diverse central projection patterns of retinal ganglion cells. *Cell Rep.* 18:2058–72

Masland RH. 2012. The neuronal organization of the retina. *Neuron* 76:266–80

McInnes L, Healy J, Melville J. 2018. UMAP: uniform manifold approximation and projection for dimension reduction. arXiv:1802.03426 [stat.ML]

Mellough CB, Bauer R, Collin J, Dorgau B, Zerti D, et al. 2019. An integrated transcriptional analysis of the developing human retina. *Development* 146:dev169474

Menon M, Mohammadi S, Davila-Velderrain J, Goods BA, Cadwell TD, et al. 2019. Single-cell transcriptomic atlas of the human retina identifies cell types associated with age-related macular degeneration. *Nat. Commun.* 10:4902

Mereu E, Lafzi A, Moutinho C, Ziegenhain C, McCarthy DJ, et al. 2020. Benchmarking single-cell RNA-sequencing protocols for cell atlas projects. *Nat. Biotechnol.* 38:747–55

Moffitt JR, Bambah-Mukku D, Eichhorn SW, Vaughn E, Shekhar K, et al. 2018. Molecular, spatial, and functional single-cell profiling of the hypothalamic preoptic region. *Science* 362:eaau5324

Ocko S, Lindsey J, Ganguli S, Deny S. 2018. The emergence of multiple retinal cell types through efficient coding of natural movies. In *Advances in Neural Information Processing Systems 31 (NeurIPS 2018)*, pp. 9389–400. N.p.: NeurIPS

O'Hara-Wright M, Gonzalez-Cordero A. 2020. Retinal organoids: a window into human retinal development. *Development* 147:dev.189746

Orozco LD, Chen H-H, Cox C, Katschke KJ Jr., Arceo R, et al. 2020. Integration of eQTL and single-cell atlas in the human eye identifies causal genes for age-related macular degeneration. *Cell Rep.* 30:1246–59

Patel G, Fury W, Yang H, Gomez-Caraballo M, Bai Y, et al. 2020. Molecular taxonomy of human ocular outflow tissues defined by single-cell transcriptomics. *PNAS* 117:12856–67

Pauly D, Agarwal D, Dana N, Schäfer N, Biber J, et al. 2019. Cell-type-specific complement expression in the healthy and diseased retina. *Cell Rep.* 29:2835–48

Peng Y-R, Shekhar K, Yan W, Herrmann D, Sappington A, et al. 2019. Molecular classification and comparative taxonomics of foveal and peripheral cells in primate retina. *Cell* 176:1222–37

Peng Y-R, Tran NM, Krishnaswamy A, Kostadinov D, Martersteck EM, Sanes JR. 2017. Satb1 regulates contactin 5 to pattern dendrites of a mammalian retinal ganglion cell. *Neuron* 95:869–83

Pollack S, Igo RP, Jensen RA, Christiansen M, Li X, et al. 2019. Multiethnic genome-wide association study of diabetic retinopathy using liability threshold modeling of duration of diabetes and glycemic control. *Diabetes* 68:441–56

Polyak S. 1957. *The Vertebrate Visual System*, ed. H Klüver. Chicago: Univ. Chicago Press
Raj B, Wagner DE, McKenna A, Pandey S, Klein AM, et al. 2018. Simultaneous single-cell profiling of lineages and cell types in the vertebrate brain. *Nat. Biotechnol.* 36:442–50
Ramani V, Deng X, Qiu R, Gunderson KL, Steemers FJ, et al. 2017. Massively multiplex single-cell Hi-C. *Nat. Methods* 14:263–66
Ramón y Cajal S. 1892. La retine des vertebres. *Cellule* 9:119–257
Rheaume BA, Jereen A, Bolisetty M, Sajid MS, Yang Y, et al. 2018. Single cell transcriptome profiling of retinal ganglion cells identifies cellular subtypes. *Nat. Commun.* 9:2759
Rodriques SG, Stickels RR, Goeva A, Martin CA, Murray E, et al. 2019. Slide-seq: a scalable technology for measuring genome-wide expression at high spatial resolution. *Science* 363:1463–67
Roesch K, Jadhav AP, Trimarchi JM, Stadler MB, Roska B, et al. 2008. The transcriptome of retinal Müller glial cells. *J. Comp. Neurol.* 509:225–38
Rosenberg AB, Roco CM, Muscat RA, Kuchina A, Sample P, et al. 2018. Single-cell profiling of the developing mouse brain and spinal cord with split-pool barcoding. *Science* 360:176–82
Saelens W, Cannoodt R, Todorov H, Saeys Y. 2019. A comparison of single-cell trajectory inference methods. *Nat. Biotechnol.* 37:547–54
Sajgo S, Ghinia MG, Brooks M, Kretschmer F, Chuang K, et al. 2017. Molecular codes for cell type specification in Brn3 retinal ganglion cells. *PNAS* 114:E3974–83
Sanes JR, Masland RH. 2015. The types of retinal ganglion cells: current status and implications for neuronal classification. *Annu. Rev. Neurosci.* 38:221–46
Sanes JR, Zipursky SL. 2010. Design principles of insect and vertebrate visual systems. *Neuron* 66:15–36
Satija R, Farrell JA, Gennert D, Schier AF, Regev A. 2015. Spatial reconstruction of single-cell gene expression data. *Nat. Biotechnol.* 33:495–502
Shekhar K, Lapan SW, Whitney IE, Tran NM, Macosko EZ, et al. 2016. Comprehensive classification of retinal bipolar neurons by single-cell transcriptomics. *Cell* 166:1308–23
Slyper M, Porter CB, Ashenberg O, Waldman J, Drokhlyansky E, et al. 2020. A single-cell and single-nucleus RNA-seq toolbox for fresh and frozen human tumors. *Nat. Med.* 26:792–802
Soneson C, Robinson MD. 2018. Bias, robustness and scalability in single-cell differential expression analysis. *Nat. Methods* 15:255–61
Sridhar A, Hoshino A, Finkbeiner CR, Chitsazan A, Dai L, et al. 2020. Single-cell transcriptomic comparison of human fetal retina, hPSC-derived retinal organoids, and long-term retinal cultures. *Cell Rep.* 30:1644–59
Srivatsan SR, McFaline-Figueroa JL, Ramani V, Saunders L, Cao J, et al. 2020. Massively multiplex chemical transcriptomics at single-cell resolution. *Science* 367:45–51
Stanley G, Gokce O, Malenka RC, Südhof TC, Quake SR. 2020. Continuous and discrete neuron types of the adult murine striatum. *Neuron* 105:688–99
Stegle O, Teichmann SA, Marioni JC. 2015. Computational and analytical challenges in single-cell transcriptomics. *Nat. Rev. Genet.* 16:133–45
Stein-O'Brien GL, Clark BS, Sherman T, Zibetti C, Hu Q, et al. 2019. Decomposing cell identity for transfer learning across cellular measurements, platforms, tissues, and species. *Cell Syst.* 8:395–411
Stoeckius M, Hafemeister C, Stephenson W, Houck-Loomis B, Chattopadhyay PK, et al. 2017. Simultaneous epitope and transcriptome measurement in single cells. *Nat. Methods* 14:865–68
Stoeckius M, Zheng S, Houck-Loomis B, Hao S, Yeung BZ, et al. 2018. Cell hashing with barcoded antibodies enables multiplexing and doublet detection for single cell genomics. *Genome Biol.* 19:244
Stuart T, Butler A, Hoffman P, Hafemeister C, Papalexi E, et al. 2019. Comprehensive integration of single-cell data. *Cell* 177:1888–902
Stuart T, Satija R. 2019. Integrative single-cell analysis. *Nat. Rev. Genet.* 20:257–72
Svensson V, Vento-Tormo R, Teichmann SA. 2018. Exponential scaling of single-cell RNA-seq in the past decade. *Nat. Protoc.* 13:599–604
Tang F, Barbacioru C, Wang Y, Nordman E, Lee C, et al. 2009. mRNA-Seq whole-transcriptome analysis of a single cell. *Nat. Methods* 6:377–82
Tasic B, Yao Z, Graybuck LT, Smith KA, Nguyen TN, et al. 2018. Shared and distinct transcriptomic cell types across neocortical areas. *Nature* 563:72–78

Tietjen I, Rihel JM, Cao Y, Koentges G, Zakhary L, Dulac C. 2003. Single-cell transcriptional analysis of neuronal progenitors. *Neuron* 38:161–75

Tran NM, Shekhar K, Whitney IE, Jacobi A, Benhar I, et al. 2019. Single-cell profiles of retinal ganglion cells differing in resilience to injury reveal neuroprotective genes. *Neuron* 104:1039–55

Trapnell C, Cacchiarelli D, Grimsby J, Pokharel P, Li S, et al. 2014. The dynamics and regulators of cell fate decisions are revealed by pseudotemporal ordering of single cells. *Nat. Biotechnol.* 32:381–86

Trimarchi JM, Stadler MB, Cepko CL. 2008. Individual retinal progenitor cells display extensive heterogeneity of gene expression. *PLOS ONE* 3:e1588

Trimarchi JM, Stadler MB, Roska B, Billings N, Sun B, et al. 2007. Molecular heterogeneity of developing retinal ganglion and amacrine cells revealed through single cell gene expression profiling. *J. Comp. Neurol.* 502:1047–65

Van der Maaten L, Hinton G. 2008. Visualizing data using t-SNE. *J. Mach. Learn. Res.* 9(11):2579–605

Van Hove I, De Groef L, Boeckx B, Modave E, Hu T-T, et al. 2020. Single-cell transcriptome analysis of the Akimba mouse retina reveals cell-type-specific insights into the pathobiology of diabetic retinopathy. *Diabetologia* 63:2235–48

van Zyl T, Yan W, McAdams A, Peng Y-R, Shekhar K, et al. 2020. Cell atlas of aqueous humor outflow pathways in eyes of humans and four model species provides insight into glaucoma pathogenesis. *PNAS* 117:10339–49

Vickovic S, Eraslan G, Salmén F, Klughammer J, Stenbeck L, et al. 2019. High-definition spatial transcriptomics for in situ tissue profiling. *Nat. Methods* 16:987–90

Vlasits AL, Euler T, Franke K. 2019. Function first: classifying cell types and circuits of the retina. *Curr. Opin. Neurobiol.* 56:8–15

Voigt AP, Binkley E, Flamme-Wiese MJ, Zeng S, DeLuca AP, et al. 2020a. Single-cell RNA sequencing in human retinal degeneration reveals distinct glial cell populations. *Cells* 9:438

Voigt AP, Mulfaul K, Mullin NK, Flamme-Wiese MJ, Giacalone JC, et al. 2019a. Single-cell transcriptomics of the human retinal pigment epithelium and choroid in health and macular degeneration. *PNAS* 116:24100–7

Voigt AP, Whitmore SS, Flamme-Wiese M, Riker M, Wiley L, et al. 2019b. Molecular characterization of foveal versus peripheral human retina by single-cell RNA sequencing. *Exp. Eye Res.* 184:234–42

Voigt AP, Whitmore SS, Mulfaul K, Chirco KR, Giacalone JC, et al. 2020b. Bulk and single-cell gene expression analyses reveal aging human choriocapillaris has pro-inflammatory phenotype. *Microvasc. Res.* 131:104031

Wang X, Allen WE, Wright MA, Sylwestrak EL, Samusik N, et al. 2018. Three-dimensional intact-tissue sequencing of single-cell transcriptional states. *Science* 361:eaat5691

Wang Z, Gerstein M, Snyder M. 2009. RNA-Seq: a revolutionary tool for transcriptomics. *Nat. Rev. Genet.* 10:57–63

Wässle H, Puller C, Müller F, Haverkamp S. 2009. Cone contacts, mosaics, and territories of bipolar cells in the mouse retina. *J. Neurosci.* 29:106–17

Wattenberg M, Viégas F, Johnson I. 2016. How to use t-SNE effectively. *Distill* 1:e2

Welch JD, Kozareva V, Ferreira A, Vanderburg C, Martin C, Macosko EZ. 2019. Single-cell multi-omic integration compares and contrasts features of brain cell identity. *Cell* 177:1873–87

Williams PR, Benowitz LI, Goldberg JL, He Z. 2020. Axon regeneration in the mammalian optic nerve. *Annu. Rev. Vis. Sci.* 6:195–213

Wolf FA, Angerer P, Theis FJ. 2018. SCANPY: large-scale single-cell gene expression data analysis. *Genome Biol.* 19:15

Wu F, Bard JE, Kann J, Yergeau D, Sapkota D, et al. 2021. Single cell transcriptomics reveals lineage trajectory of retinal ganglion cells in wild-type and Atoh7-null retinas. *Nat. Commun.* 12:1465

Yamagata M, Yan W, Sanes JR. 2021. Cell atlas of the chick retina: single cell profiling identifies 136 cell types. *eLife* 10:e63907.

Yan W, Laboulaye MA, Tran NM, Whitney IE, Benhar I, Sanes JR. 2020a. Mouse retinal cell atlas: molecular identification of over sixty amacrine cell types. *J. Neurosci.* 40:5177–95

Yan W, Peng Y-R, van Zyl T, Regev A, Shekhar K, et al. 2020b. Cell atlas of the human fovea and peripheral retina. *Sci. Rep.* 10:9802

Yi W, Lu Y, Zhong S, Zhang M, Sun L, et al. 2020. A single-cell transcriptomic atlas of the aging human and macaque retina. *Nat. Sci. Rev.* 8:nwaa179

Young RW. 1985. Cell differentiation in the retina of the mouse. *Anat. Rec.* 212:199–205

Yu C, Saban DR. 2019. Identification of a unique subretinal microglia type in retinal degeneration using single cell RNA-seq. *Adv. Exp. Med. Biol.* 1185:181–86

Yuste R, Hawrylycz M, Aalling N, Aguilar-Valles A, Arendt D, et al. 2020. A community-based transcriptomics classification and nomenclature of neocortical cell types. *Nat. Neurosci.* 23:1456–68

Zeng H, Sanes JR. 2017. Neuronal cell-type classification: challenges, opportunities and the path forward. *Nat. Rev. Neurosci.* 18:530–46

Zheng GX, Terry JM, Belgrader P, Ryvkin P, Bent ZW, et al. 2017. Massively parallel digital transcriptional profiling of single cells. *Nat. Commun.* 8:14049